ADVANCED ENGINEERING MATERIALS
www.aem-journal.com

Advances in Hybrid Icing and Frosting Protection Strategies for Optics, Lens, and Photonics in Cold Environments Using Thin-Film Acoustic Waves

Hui Ling Ong, Zhangbin Ji, Luke Haworth, Yihao Guo, Jaime del Moral, Stefan Jacob, Ana Borras, Agustin R. Gonzalez-Elipe, Jikai Zhang, Jian Zhou,* Glen McHale, and Yong-Qing Fu**

Fogging, icing, or frosting on optical lenses, optics/photonics, windshields, vehicle/airplane windows, and solar panel surfaces have often shown serious safety concerns with hazardous conditions and impaired sight. Various active techniques, such as resistive heating, and passive techniques, such as icephobic treatments, are widely employed for their prevention and elimination. However, these methods are not always suitable, effective, or efficient. This review provides a comprehensive overview of the fundamentals and recent advances of transparent thin-film surface acoustic wave (SAW) technologies on glass substrates for monitoring and prevention/elimination of fogging, frosting, and icing. Key challenges related to fogging and icing on glass substrates are discussed, along with fundamental mechanisms that establish thin-film SAWs as optimal solution for these issues. Various types of thin-film acoustic wave technologies are discussed, including recent wearable and flexible SAW devices integrated onto glass substrates for expanding future applications. The focus of this review is on the principles and strategies for hybrid or integrated de-fogging/de-icing and sensing/monitoring functions. Finally, critical issues and future outlooks for thin-film-based SAW technology on glass substrates in industry applications are presented.

1. Introduction

Glass is commonly utilized in windows, mirrors, lenses, and optics,[1–4] with merits of relatively low-temperature coefficient of frequency, good optical transparency, and high light transmission performance (>80%).[1,5–7] Major issues in cold environments for glass-based components include fogging, condensation, icing, and frosting, particularly in high humidity and water condensation conditions, with surface temperatures at or below the dew point.[8–15] For example, significantly reduced vision, foggy, or smog conditions pose great risks to safety and health, compromising people's travel ability and overall well-being.[16–19] Severe weather conditions often lead to the build-up of condensation, ice, and snow on the surfaces of lenses, optical components, and photonic devices.[20] This can lead to unwanted changes in optical properties, poor operability, and severe safety risks.[8,11] On another matter, efficiency/performance of the photovoltaic

H. L. Ong, L. Haworth, J. Zhang, Y.-Q. Fu
Faculty of Engineering and Environment
Northumbria University at Newcastle
Newcastle upon Tyne NE1 8ST, UK
E-mail: richard.fu@northumbria.ac.uk

Z. Ji, Y. Guo, J. Zhou
College of Mechanical and Vehicle Engineering
Hunan University
Changsha 410082, China
E-mail: jianzhou@hnu.edu.cn

The ORCID identification number(s) for the author(s) of this article can be found under https://doi.org/10.1002/adem.202402139.

DOI: 10.1002/adem.202402139

J. del Moral, A. Borras, A. R. Gonzalez-Elipe
Nanotechnology on Surfaces and Plasma Lab
Materials Science Institute of Seville
Consejo Superior de Investigaciones Científicas (CSIC)
Americo Vespucio 49, 41092 Sevilla, Spain
E-mail: anaisabel.borras@icmse.csic.es

S. Jacob
Acoustics and Mechanics
German National Metrology Institute (PTB)
Bundesallee 100, 38106 Braunschweig, Germany

G. McHale
Institute for Multiscale Thermofluids
School of Engineering
The University of Edinburgh
Edinburgh EH9 3FD, UK

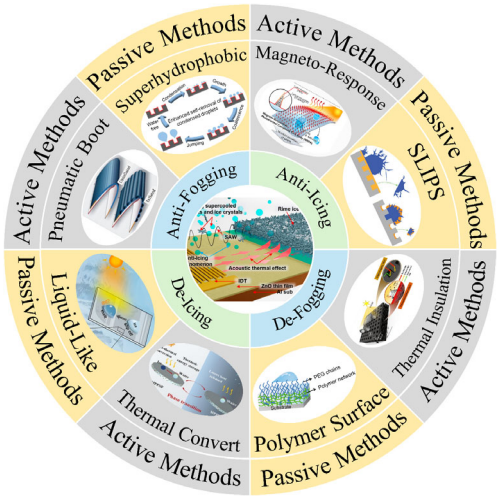

Figure 1. Hybrid active and passive technologies for fogging and icing mitigation applications on glass.

(PV) modules and power generation systems such as wind turbines or cables become deteriorated when fogging, frost, and ice gradually build up on their surfaces.[8,21–25]

As illustrated in **Figure 1**, numerous passive (e.g., surface modifications or coatings) and active (e.g., energetic or chemical activation) strategies have been applied to minimize surface accretions brought on by fogging, frosting and icing. Taking fogging as an example, there are different approaches for its removal, which can be classified as warm or cold fog elimination.[16,17,26–28] Fogging happens quickly at temperatures over 0 °C (known as warm fogging), and the procedures for removal generally need external energy methods, such as heating, or dynamic perturbation i.e. mechanical methods. Alternative passive anti-fogging methods rely on seeding hygroscopic particles[16,17,26–28] and employing photothermal plasmonic approaches.[29,30] When the temperature falls below 0 °C, cold fogging becomes dominant and mostly consists of water droplets, which usually result in a phase change in the fog (e.g., the formation of ice crystals in fog).[16,17,19] One typical active approach to dealing with cold fog is to utilize refrigerants, which are detrimental to the environment.[16,17,26–28] Many other active methods of fog removal, such as localized electrothermal heating, tend to have poor efficiency and large power consumption or represent pollution issues.[16,27]

Using superhydrophobic and icephobic surfaces to lower solid surface energy and water–ice adhesion is one of the most significant passive anti-icing strategies, as shown in Figure 1.[15,31–33] It has been demonstrated that in comparison to hydrophilic or neutral wetting surfaces, superhydrophobic surfaces (SHS) with large contact angles significantly postpone droplets' freezing on the surface substrate.[14,15,32,34] Unfortunately, in addition to their poor mechanical and adhesive issues, these superhydrophobic layers have potential durability issues.[35–37] A number of functional treatments, some of which are often used for glass surfaces, have been studied in the past for ice mitigation.[38–41] However, the use of these surfaces does not always seem to reduce ice adhesion or improve icing protection or to provide a long term performance.[42]

Figure 1 also shows active de-icing techniques utilizing external energy sources such as heating, mechanical vibrations, pneumatic boots, and ultrasonic waves.[43,44] However, ice mitigation using these technologies sometimes needs a significant amount of energy or is difficult to apply to substrates such as glass.[45] One of the key challenges of mitigation methods on glass is that most passive or active methods could affect the optical performance of the components. Another critical issue is that many active or passive methods, such as mechanical, chemical, or electrical methods,[25] increase the risk of glass fracture, may damage the surfaces of optical components, or increase the surface roughness of glass, all of which have negative influences on mitigation efforts or compromise the optical properties of the transparent material.[46,47] Therefore, it is essential to look for alternative ice mitigation methods to apply ice protection measures in a manner that is highly effective and environmentally benign.

Because of its many benefits, surface acoustic wave (SAW) technology has recently emerged as a suitable active methodology, with extensive applications in microfluidics, sensing, communications, medical, and lab-on-a-chip (LOC).[48–51] SAW-based microfluidics are effective in fulfilling pumping, jetting, nebulizing, and manipulating liquid media and microparticles inside liquids.[52–54] SAW sensing has been widely applied for monitoring physical, chemical, and biological variables, including respiration/breath detection, optical/light sensing, gas sensing, humidity sensing, and ultraviolet (UV) sensing.[50,55,56] It has also been recently reported for fogging and icing detection.[48,57] Applying SAWs can significantly lower operation costs and system complexity due to advantages such as integration, remote/wireless functions, and effectiveness.[58–62] With respect to other active de-icing methods (see Figure 1), excitation by SAW presents potential advantages in terms of a more straightforward integration onto glass substrates, little energy consumption, easier processability, and the possibility to provide both sensing and actuation functions, enabling a smart actuation mode independent on human intervention.

Most acoustic wave (AW) devices are made of bulk piezoelectric materials. However, they are often expensive, tedious to fabricate or operate, and challenging for microelectronics and optics integration.[55,63] Moreover, they become exceedingly fragile and weak when polished into thin and small structures for certain applications, such as high-frequency and flexible ultrasonic devices.[55,64] Recently, piezoelectric thin films-based SAW devices, such as those integrating zinc oxide (ZnO), aluminum nitride (AlN), or lead zirconate titanate (PZT), have been thoroughly studied for various applications.[55,59] These piezoelectric film-based SAW devices can be readily produced on glass substrates to form transparent AW structures and provide disposable, bendable/flexible acoustofluidics or sensing devices,[53,55] as well as integrated systems such as LOCs.[53,55]

Currently, there have been some initial studies using active methods including thin-film SAWs on aluminum substrate or bulk ceramic of lithium niobate ($LiNbO_3$) for anti-fogging and de-icing purposes.[65–71] However, few studies have been focused on using thin-film-based SAW devices on the glass substrates for these applications.[71,72] For potential optics and window applications, there are also other transparent substrates commonly used, including plastics, composites, or laminates. However, this

review article will focus on glass substrates because sound transmission on those other substrates is not as effective due to the severe wave energy dissipation.[73] There are many key issues for these thin-film SAW technologies on the glass substrates, including elucidation of mechanisms of de-fogging or de-icing on glass, compatibility of passive methods such as a hydrophobic surface treatment with SAWs, and its efficiency, effectiveness, scalability, and industry scale production.[72]

This review article summarizes the principles of thin-film AWs, SAW sensing, and acoustofluidics on glass substrates for anti-fogging and anti-/de-icing techniques. Firstly, we outline the main difficulties and challenges posed by the fogging and icing problems on glass substrates, describing basic principles of current technologies applied for this purpose, and reviewing how thin-film SAWs are used in these situations. Next, we explore possible applications of these thin-film devices on glass, introducing recently developed wearable and flexible transparent SAW devices. Different thin-film AW modes generated on the glass substrates are explained. Further discussions are primarily concentrated on the ideas and strategies for de-fogging and de-icing, along with the sensing and monitoring methods utilized in industry practices. Finally, the key issues and potential uses of thin-film-based SAW devices on glass substrates for icing and fogging applications are discussed for future prospects.

2. Fundamentals of Strategies for Preventing Fogging/Icing on Glass

2.1. Passive Technologies for Fogging and Icing Issues on Glass

Passive technologies are aimed at modifying the surface properties of glass to either delay the ice formation when supercooled water droplets are impinging onto the surface or decrease the ice adhesion strength once ice aggregates are formed on the surface. There is not a unique strategy to promote any of these functions. Some procedures entail the modification of wetting properties of the glass surfaces to make them hydrophobic or superhydrophobic. However, superhydrophobicity is not always synonymous with efficient icephobicity.[74,75] From a physical point of view, the common approach applied is to decrease the surface energy or ice adhesion on the glass substrate. In general, modifying the surface roughness and/or tailoring the surface composition are two strategies to achieve some of these properties and functionalities.

Various passive fogging protection techniques, especially those integrating micro- and nanoscale textures with different levels of wettability and hygroscopic patterns, have been commonly applied to enable frost-free or easy frost removal surfaces without the need for additional energy supplying methods. They primarily consist of the modification of surface micro- and nano-structures and/or material's intrinsic properties.[76] Furthermore, some passive anti-/de-icing techniques offer advantages such as nontoxic nature, simplicity of use, reduction of weight, and downsized equipment requirements.[76] In addition, several types of surfaces have shown great potentials for ice mitigation, for example, surfaces that aid in the separation of accumulated ice; surfaces that postpone ice accumulation; and surfaces that thwart the accumulation of ice formation.[77]

SHS based on nanoscale features on microscale structures have been explored for achieving good icephobicity.[78–80] Building upon SHS, slippery liquid-infused porous surfaces (SLIPS) show both ultralow ice adhesion and enhanced anti-icing performance.[81–83] Various polymer coatings have been explored in terms of their anti-icing capabilities.[84] Further research on using polymer surfaces to reduce ice adhesion has been focused on block copolymers, grafting of elastomers and fluorinated coatings.[85–89] Recently there has been a transition from perfluorinated molecules (due to their potential environmental impact and toxic fabrication methods[90]) into others such as smooth PDMS-based coatings. These include the use of PDMS surfaces from methylated and nonmethylated surfaces, lubricant-infused PDMS brush structures, crosslinked PDMS structures, PDMS-loop structures of varying chain lengths, and PDMS brushes imbibed with toluene vapor.[91–95]

2.1.1. Icephobic Surfaces or Coatings on Glass

Ice formed on glass can be classified into two groups, namely glaze (or transparent) ice and rime rice, based on their morphologies and densities.[43,45,96–98] Mostly as a result of rapid ice formation or supercooled and high-humidity settings, rime ice possesses specific properties, including porous microstructure, low density, high opacity, and loose adhesion onto the structural surfaces.[31,43,96,99] Glaze ice, on the other hand, is smoother, more compact, more closely packed, and has a higher surface adhesion to most substrates than rime ice.[31,45,96,99] Glaze ice develops when the temperature is relatively high, i.e., slightly below the freezing point.[15,43,45] It is normally heavier and adheres more strongly to the glass surface as compared to rime ice which is much lighter and fluffier on the glass surface. The key parameters controlling the different types of ice formation include supercooling conditions, surface conditions and temperatures, cooling speeds, and relative humidity.[31,99] It is also worth noting that the results of de-icing can be easily extended to fogging conditions. However, the opposite is not so straightforward, as the volume of accreted ice and its effect on performance are more critical for rime and glaze ice than for fogging. Additionally, a high ice adhesion of surfaces hinders de-icing, either through active or passive methods. Generally, a high surface roughness of the substrates contributes to an increase in ice adhesion, while roughness is a requirement for superhydrophobicity or hydrophilicity, two conditions which favor water sliding and therefore anti-fogging behavior.

Reducing glass's surface energy and water–ice adhesion using icephobic functionalization (see **Figure 2**) is regarded as one of the key passive anti-icing strategies.[15,31–33,95] The freezing process of a droplet can be significantly slowed down by forming a SHS as opposed to a droplet frozen on a hydrophilic surface.[14,15,32,34] There are reports for delaying freezing on hydrophilic surfaces or SLIPS with hydrophilic lubricants.[83,100] Extensive studies have been performed using different functional icephobic glass surfaces for ice mitigation.[38–41]

Various organic and polymer-based surface treatments have been applied for anti-icing regarding both glaze and rime ice. For example, polyhedral oligomeric silsesquioxane (POSS) is one of the most commonly used. The inorganic core of POSS

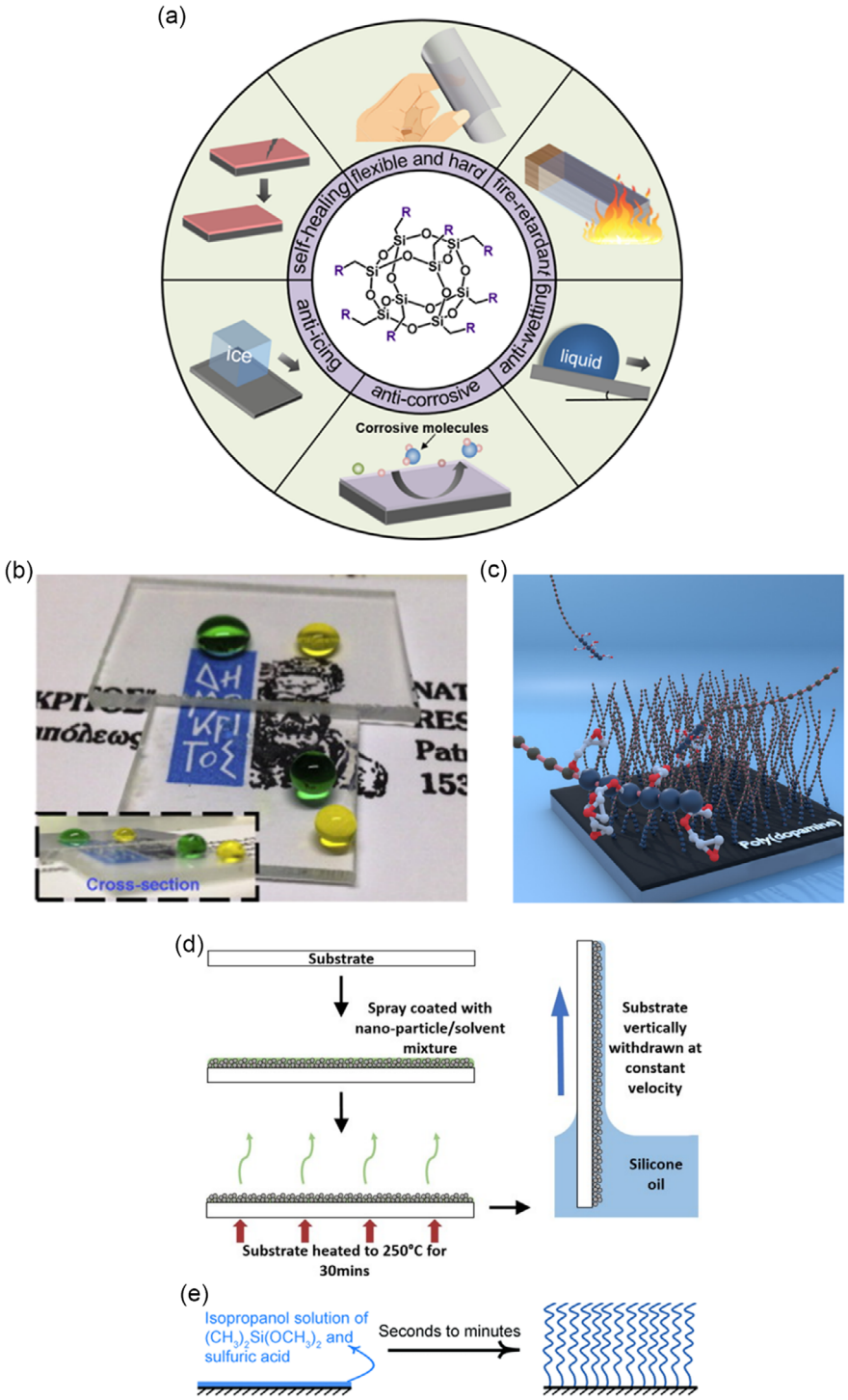

Figure 2. Icephobic and fogging-resistant micro- and nanostructure designs on glass substrates. a) Polyhedral oligomeric silsesquioxane (POSS) molecules' hybrid organic–inorganic nanostructure and its uses in the coatings industry such as self-healing materials, icephobic coatings, hard and flexible coatings, anti-wetting surfaces, and fire-retardant coatings. Reproduced (Adapted) with permission.[101] Copyright 2024, John Wiley & Sons-Books. b) Illustration of liquid droplets on untreated (top) and treated (bottom) samples, whereby they are spherical and have a tendency to roll on the treated sample, while they spread on the untreated sample (see droplet reflection on the substrate). Reproduced (Adapted) with permission.[108] Copyright 2024, Elsevier. c) Illustration of a simple, modular two-step grafting method that may be used to introduce desired functional polymer brushes onto a wide variety of substrates with varying chemical compositions.[111] d) Fabrication process of SLIPS via spray coating with a nanoparticle/solvent mixture from top to bottom in one pass, followed by heating process and dip coating with silicon oil.[115] e) Acid-catalyzed graft polycondensation of dimethyldimethoxysilane to produce omniphobic surfaces that are robust at high temperatures and stable under pressure. Reproduced (Adapted) with permission.[118] Copyright 2024, John Wiley & Sons-Books.

(see Figure 2a) is a 3D nanosized cage with alternating Si—O bonds, where the organic functional groups are covalently bonded onto the Si vertices.[101] Because of their special structures, they can be combined with certain types of polymers in a variety of ways, such as chemical crosslinking, covalent grafting, and physical mixing.[101] Additionally, the POSS's hybrid inorganic/organic structure provides the coating materials with the desired mechanical, icephobic, anti-wetting, anti-corrosive, and fire-retardant functionalities.[101]

Another common method is to apply the cyclic fluoropolymer, or cyclic transparent optical polymer (CYTOP, Asahi Glass Co.), which has been used to lower the surface energy and prevent contamination or other apparent damages.[102,103] It provides a smooth, amorphous, and relatively durable hydrophobic surface.[103,104] CYTOP has randomly orientated and fixed polymer chains. Due to its strong dipoles induced by the carbon-fluorine bonds, it can prevent charge trapping on semiconductor substrates and offer a superior electrical and chemical stability.[103,104]

Various surface treatments using plasma[105] or physical or chemical vapor depositions have been used for fabrication of fluorocarbon polymers that present a high versatility for the control of the fluorine contents and types of —CFx functional groups in the polymer.[106,107] Using plasmas, Kontziampasis et al.[108] created nanoscale anti-reflective (nanoAR), superhydrophobic, superoleophobic PMMA-coated glass as shown in Figure 2b. They used O_2 plasma for etching and nanotexturing to create the required topography on the PMMA surfaces and increase the nanoAR's performance, followed by the vacuum deposition of a perfluorinated self-assembled monolayer to induce hydrophobicity.[108] Their findings indicated that a plasma processing period of around 150 s gave rise to an optimal shape topography for an effective icing protection.[108] Although nano-/microtexturing is good for delaying ice accretion, it could be detrimental for ice adhesion in many cases. Meanwhile, once an active AW de-icing was implemented, the hydrophobicity helps to reduce the energy requirements in the micro- and nanoscale levels.[108]

Hydrophobicity and low surface energy are the key characteristics of these polymeric coatings that have shown clear enhancement of the anti-icing properties.[109] Similar effects can be achieved when grafting certain fluorocarbon molecules onto the surface of glass. The resulting surface tethered molecules provide a good hydrophobicity and contribute to the decreased ice nucleation capacity on the surface, thus increasing the freezing delay time and reducing the ice adhesion stress. Among them, 1H,1H,2H,2H-perfluorooctyltriethoxysilane is one of the most widely used fluorinated molecules to modify the surface properties of oxide surfaces.[89] It is tightly anchored on the surface by the reaction of the ethoxy silane groups with the hydroxyl groups on the substrate surface. Its use is widespread to modify the wetting properties of substrate and particle surfaces of different materials, including glass.[110] For example, a remarkable increase in wetting angles was reported from about 50° for the bare glass substrates to values higher than 100° for the grafted surfaces.[110] However, we should mention that currently there are great environmental and health concerns for these fluorocarbon-based treatments or per- and polyfluoroalkyl substances (PFAS), which are often called "forever chemicals." There are legal and regulatory frameworks to ban or remove the use of these PFAS and therefore, their alternatives are currently major focused research topics.

Polymer brush coatings are arguably among the most effective surface modification methods because their special structures can be tailored down to nanometers (see Figure 2c).[111] Polymer brushes can be fabricated with various surfaces and monomer functionalities.[111] For example, Teunissen et al.[111] applied a grafting technique on glass and used a radical addition–fragmentation chain transfer polymerization method, producing different block copolymers. Each of these includes a short poly(glycidyl methacrylate) (poly(GMA)) segment to be attached to the amine groups in the poly(dopamine) film, thus achieving various types of hydrophobicity.[111] Zhou et al.[112] produced a zwitterionic hydrophilic polymer brush coating using UV-induced grafting polymerization of methacryloxyethyl sulfobetaine monomer on salinized glass and demonstrated exceptional anti-fogging, anti-frosting, and self-cleaning properties.[112] This polymer brush coating on glass exhibited excellent abrasion, durability, and water resistance, that is the essential requirements for an anti-fogging coating to work consistently and durably.[112]

Another commonly studied method is to utilize hydrophobic SLIPS, as shown in Figure 2d. These coatings consist of a lubricating liquid film infused into a fixed surface modified structure (micro-, nano-, or both) on a substrate.[81,83,100,113] The result is an interface suitable for liquid–liquid contact and a virtually smooth surface at the molecular level. For effectively preventing surface damage, these SLIPS treatments usually offer a self-healing mechanism.[75,114] To restore the damaged region for the SLIPS, the liquid lubricant is able to flow,[115–117] thus maintaining the overall liquid–liquid surface interactions.[118–120] The SLIPs can be formed, either by incorporating a porous layer directly on glass (where the porous layer has to be preferentially wetted by the lubricant oil and then infused with oil or other liquid) or simply etching the glass substrate (which can form micro- or nanoscale porous structures and then to convert them into hydrophobic for the lubricant liquid to infuse easily inside). A very common and popular slippery liquid used for infusion is Krytox from Dupont, a fluorine-containing compound widely used for these applications due to its high stability and low surface energy in liquid form.[121] However, as mentioned before, the new environmental regulations have been focused on stopping/decreasing or in the medium term suppressing or lowering the uses of fluorine-containing compounds. Therefore, alternatives are urgently needed to replace all these fluorinated coatings, using fluorine-free slippery liquids, such as silicone oil or polymer mixtures,[122,123] or drastically decrease the amount of fluorine compounds. Within this last approach, aforementioned strategies are used to modify the wetting and icing functionalities of the surfaces, namely, covering the substrates with a very thin layer of a hydrophobic fluoropolymer[109] or grafting short fluorocarbon chains on the substrate surface.[124]

Another recently investigated method that does not use fluoropolymers consists of "liquid-like" icephobic layers or coatings, such as a nanoscale slippery omniphobic covalently attached liquid (SOCAL) surface. The SOCAL coating uses flexible short polydimethylsiloxane (PDMS) chains covalently bonded onto the substrate to provide liquid-like characteristics.[118,125] The PDMS tethered molecules exhibit behaviors akin to those of

liquid-infused surfaces or network materials infused with liquid lubrication.[126] On the other hand, the PDMS chains with nanoscale structures of tethered molecules of SOCAL (Figure 2e) are quite flexible and tuneable, providing SOCAL coatings with remarkable icephobic qualities.[66,118,125,127–130]

2.1.2. Microstructured and Nanostructured Surfaces

Dual-scale or micro- and nanostructured surfaces are known to provide a reduced contact area for impinging water droplets and low roll-off angles, making those SHS attractive as anti-icing and anti-fogging solutions. These functions stem from the combination of multiscale roughness levels and low surface energy.[114] Nevertheless, these superhydrophobic micro-/nanostructured surfaces have frequently shown issues of poor durability, limited long-term stability, little mechanical robustness upon adhesion, light scattering, and a high dependence on feature size or even sustainability.[35–37,131]

Photolithography[132] and soft lithography, as well as replication nanoimprinting processes,[133] have been widely employed to fabricate micro- and nanopatterns for anti-icing and anti-fogging applications, particularly for bioinspired approaches employing polymeric surfaces.[134] However, these procedures usually require highly specialized facilities and are challenging to scale up at reasonable costs. A more affordable approach has recently emerged based on the wrinkling effects appearing on stretchable polymers such as PDMS. Thus, microscale patterns can be created on the surface of the polymer upon elongation, while upon prestretching and further surface modifications, superhydrophobic, anti-icing, highly resilient, and transparent coatings, well adapted for PV panels, can be produced.[135]

From a practical point of view, the fabrication of nanopillars (NPs) and similar well-ordered patterned structures on glass surfaces faces obvious shortcomings when considering the modification of large surface areas. In such a scenario, versatile laser-based procedures are advantageous for the scalable micro- and nanostructuring of various materials. Controlling wettability, freezing delay, anti-icing response, anti-bacterial activity, or anti-fouling capacity are some of the effects pursued by these laser micromachining methods. However, the direct laser micromachining of glass surfaces is often a time-consuming and costly procedure[136,137] and may induce surfaces with high light scattering and, therefore, loss of transparency. Alternatively, to reduce such effects and enhance water removal and anti-icing capacity, the laser-structured glass substrates are further modified by grafting organic molecules conferring specific hydrophobic properties.[138] The advent of ultrashort pulsed lasers is opening new glass modification approaches. For example, Yalikun et al.[139] employed a femtosecond laser to create various microstructures in a large range of shapes and sizes on ultrathin glass substrates to produce flexible glass microfluidic chips.[139] Lee et al.[140] made millimeter-scale through-holes using helical cutting of a variety of glass materials. Such femtosecond laser helical drilling has also been used to process considerable areas of glass with a good aspect ratio and selectivity.[140] In this context, Cao et al.[141] modified the laser beam process parameters, such as feed rates, voltage, rotational speed, pulse on/off-time ratio, and electrolytes concentration in the laser drilling and milling processes to process various microstructures on the Pyrex glass.

Many other approaches have aimed at fabricating micro- and nanostructured surfaces incorporating NPs and integrated patterns fabricated by scalable methods. For example, a unique process of passive radiative cooling was introduced by Chillon et al.[142] which was based on the scalable manufacturing of silica NPs on glass substrates such as fused silica (FS). They demonstrated that the NPs' visible optical range haze might be eliminated by a thin polymer coating embedded in them, improving optical transmission and enabling a design compatible for use in optical screens.[142] Yu et al.[143] also presented a unique nonlithographic technique, which used a reactive plasma treatment and a sacrificial SiO_2 layer to create silica nanostructures directly on glass. Since the SiO_2 nanoscale pillars acted as shadows to avoid the continuous plasma etching of the glass substrate underneath, the glass surfaces underwent a nanostructured growth consisting of nanopatterns.[143]

Wang et al.[144] reported self-responsive surfaces as those widely observed in natural organisms and systems such as earthworms and poison dart frogs, whose secretion glands under their skin release lubricants to form a slippery layer. The surface lubrication is achieved by an underskin pressure or concentration gradient that has inspired the designs of anti-icing surfaces with embedded lubricants in the substrate. They have also created a self-responsive substrate, which was developed through phase separation or dissolving urea and polydimethylsiloxane (PDMS) copolymers and excess silicon oil into tetrahydrofuran and then trapping the excessive silicone oil as internal droplets using the crosslinked polymer matrix. They reported that icephobic surfaces following such a strategy with the surface regenerable lubricant layers achieved an ice adhesion strength below 40 kPa. Besides these small liquid oil molecules, solid lubricants could also be used in self-responsive surfaces to regenerate surface lubricating layers and facilitate ice removal.[144] Ahmad et al.[145] reported the preparation of an anti-reflective coating with anti-icing properties that possessed a good thermal stability and the ability to mitigate ice formation.

Although glass microstructures can be readily achieved in various ways, using the previously mentioned procedures at an industrial scale and for practical applications is complex and challenging. It requires sophisticated control techniques, expensive processing equipment, and overcoming the usual limited material removal rates of these methods.[146]

2.2. Various Types of Active Methods as De-icing Strategy on Glass

Applications of external energy sources, such as heating, mechanical vibrations and ultrasonic waves, are other key active strategies for icing protection.[43,44,147] In the following section, various types of active methods such as electrothermal, photothermal, or ultrasonic/AW methods are discussed.

2.2.1. Photothermal Methods

Figure 3 illustrates key examples of photothermal methods for icing and fogging protection functions. Photothermal coatings

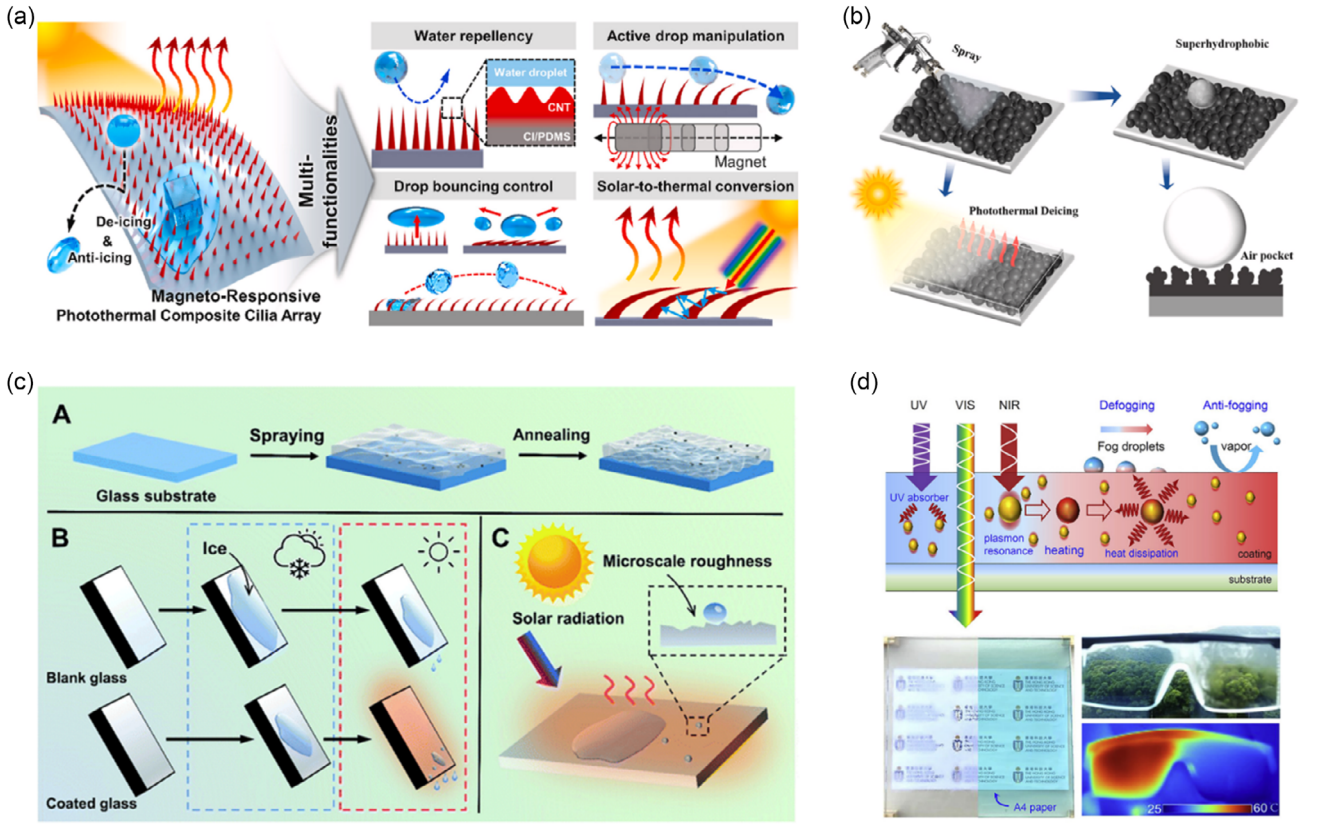

Figure 3. Photothermal methods for de-fogging, anti-fogging, de-icing, and anti-icing functions. a) Multifunctionalities of the MRPA. Reproduced (Adapted) with permission.[147] Copyright 2024, Elsevier. b) A superhydrophobic photothermal coating fabricated on a glass substrate via a two-step spraying technique where the coating demonstrated exceptional functionalities such as superhydrophobicity, strong photothermal effect, strong chemical and mechanical stability, and outstanding anti-icing/active de-icing and de-frosting properties. Reproduced (Adapted) with permission.[148] Copyright 2024, Elsevier. c) A schematic illustration showing how transparent, hydrophobic, and photothermal coating was prepared, the principles of photothermal and regular glass anti- and de-icing procedures, and a scheme of photothermal glass de-icing mechanism.[151] d) Illustration of the highly transparent, photothermally selective coating, based on solution-processed cerium-doped tungsten trioxide nanoparticles for anti- and de-fogging functions. Reproduced (Adapted) with permission.[20] Copyright 2024, Elsevier.

have a good capability to accelerate the melting of ice on the surface and promote the roll off from the glass surface.[148] Various photothermal methods, based on plasmonic materials, have been developed recently where photon energy is converted into thermal energy via light absorption and scattering mechanisms.[149,150] For example, multifunctional magnetoresponsive photothermal composite cilia arrays (MRPAs) were proposed by Lee et al.[147] accomplishing impressive anti- and de-icing properties as presented in Figure 3a. They found that the MRPA achieved instantaneous and reversible structural actuation motions in the presence of an external magnetic field and retained good superhydrophobicity.[147] The MRPA has the ability to prevent, postpone, and eliminate ice formation from supercooled impinging and stationary droplets, as demonstrated by its multifunctional features shown in Figure 3a.[147] He et al.[148] presented a superhydrophobic coating with photothermal action to enhance anti-icing, de-icing, and de-frosting capabilities. They reported that the coating exhibits strong chemical and mechanical stabilities, good photothermal response (e.g., the surface temperature of the obtained coating was quickly increased to 111.8 °C under one sun), and outstanding superhydrophobicity (with a water contact angle of 155° and a sliding angle of 4°).[148] The coating exhibited outstanding anti-icing, de-icing, and de-frosting properties as shown in Figure 3b[148] and effectively delayed ice accretion or freezing.[148] A highly transparent and photothermal composite coating was also prepared on glass surfaces by Guo et al.[151] employing a direct-spraying sol technique and Cu_7S_4 nanoparticles and organosilicone sols to achieve good photothermal conversion and hydrophobic properties, demonstrating an outstanding anti-icing and self-melting ice performance as shown in Figure 3c.[151]

However, there are issues for utilizing photothermal methods. For instance, many of these photothermal nanomaterials cannot be directly formed as a hierarchical structured surface for light capture without the inclusion of polymer binders.[152] Furthermore, even though photothermal surfaces can be used for de-icing, their efficiency in icing delay is frequently small at low temperatures.[152] Moreover, for practical outdoor applications, photothermal efficiency is very dependent on solar irradiation intensity and therefore highly dependent on environmental conditions and day times (e.g., substrate temperature, presence of clouds, night, etc.). The use of artificial lighting might be an

option, but its practical implementation is not realistic in most cases. Most photothermal anti- and de-icing surfaces with hierarchical structures have shown shortcomings such as difficulties in preparation, strong dependence on environmental lighting conditions, difficulty for practical applications and poor durability.[152]

As addressed above, surface fogging produces a number of issues in daily life and decreases the light transmission of optically clear materials such as in eyewear, windows, and displays.[20,29] Energy-neutral and passive methods, which are primarily dependent on surface wettability engineering, are often hampered by nonuniformity, pollutant deposition, and a lack of resilience, hazards that significantly reduce their performance and durability.[20,29] Recently, transparent photothermal materials have come to light as a sustainable and environmentally friendly option to reduce surface fogging.[20,29] Nevertheless, the majority of these photothermal materials solely utilize the solar energy's broadband spectrum, and the spectral characteristics are still needed of adjustment for simultaneously maximizing both photothermal impact and visibility.[20]

Li et al.[20] fabricated a transparent and photothermally selective coating using solution-processed tungsten trioxide nanoparticles doped with cerium. They reported that under one-sun illumination, this coating achieved a temperature increase of 38 °C and a high absorption of UV and near-infrared light of more than 90%.[20] This resulted in remarkable anti-fogging and de-fogging abilities under extremely frigid or humid conditions as presented in Figure 3d.[20] Extensive intricate surfaces coated with photothermal materials are utilized in both long-term durability and field anti-fogging experiments, demonstrating their considerable potential for anti-fogging applications.[20]

Haechler et al.[29] fabricated a transparent and photothermally activated covering layer which reacts to sunshine. Such metamaterial coating retains a visual transparency because it has a nanoscopically thin percolating gold layer with a maximum abosrption in the near-infrared region.[29] When compared to uncoated samples, the photoinduced heating effect allows for prolonged and improved fog prevention (up to four times better) and increased removal efficiency (up to three times better), as well as an overall outstanding performance for both indoor and outdoor conditions, even in foggy situations.[29] Because of its extreme thinness (≈10 nm), the coating can be integrated beneath other coatings and is durable even on extremely compliant substrates.[29] It can be fabricated using ordinary, easily scaled manufacturing procedures.[29]

2.2.2. Electrothermal Methods

The principle of electrothermal de-icing systems consists of applying the heat generated from electrical energy to increase the ice/substrate contact temperature above the freezing point. This causes a thin liquid layer to be formed at the interface, which helps to accelerate the de-icing process by reducing the ice layer's adhesion to surfaces.[153] Rapid heating is made possible by the electrothermal activation and effectively enables de-icing and anti-icing functions. Electrothermal de-fogging and de-icing are costumary in automobile rearview windows where these functions are induced by Joule dissipation of the electrical current passing through resistive heating wires. New developments incorporate embedded layers or thin films as heating elements. A basic requirement is that the thin films used as resistors are transparent. Solutions based on indium tin oxide (ITO) and fluorine-doped tin oxide (FTO) alone or incorporating silver-based nanowires are currently used for such architectural layered designs. An overview of these procedures and other glass modification technologies to improve its performance in buildings can be found in ref. [154], where the relative efficiencies of metal-based, carbon-based, and hybrid metal/carbon composites are compared. Glass and other transparent and flexible materials (i.e., polymers) have also been used as substrates to incorporate these electrothermal coatings. It is noteworthy that the approaches utilized for building glass are perfectly scalable to large areas and use robust and low-cost technologies. Among the solutions proposed, carbon nanotubes (CNTs) (**Figure 4**a)[155] and graphene (Figure 4b)[156] are popular materials used as heating elements. Graphene has particularly attracted much attention for the fabrication of high-performing electrothermal defoggers and anti-icing coatings as shown in Figure 4c.[157]

Wang et al.[158] recently merged electrothermal and photothermal activation in a PDMS matrix composite coating, presenting superhydrophobicity and a high passive anti-icing capacity due to its NP structure as shown in Figure 4d. In this design, CNTs and titanium nitride (TiN) nanoparticles were incorporated in the PDMS matrix to provide both electrothermal and photothermal de-icing functionalities. However, since the transparency of these types of coatings on glass could be a concern, authors[159] further developed a series of coatings where the PDMS brushes were grafted in an epoxy matrix with near-infrared (NIR) and UV absorbers. The electrothermal function was provided by an ITO layer deposited on top of the glass. A maximum visible light transmission up to 77% was achieved, while prominent anti-icing and water slippery capacities similar to those of typical SLIPS were achieved.

Electrothermal activation has also been combined with superhydrophobic coatings[160] to achieve significant reductions of energy consumption. Although the anti-icing effect of the SHS in terms of energy savings was insignificant on its own, Sun et al.[161] found that when combined with an electrothermal procedure to heat the system up to 15 °C, 76.7% of the energy required for anti-icing could be saved.[161] However, electrothermal procedures still face different issues due to the need of integration of circuit elements for heating and their high energetic demands, very often resulting in poor energy efficiency and low operating effectiveness.

2.2.3. Ultrasonic and Acoustic Wave Methods

In the context of this review, it is important to differentiate between ultrasonic waves with frequencies either smaller or larger than a few MHz. Low-frequency AWs are commonly produced using bulk piezoelectric generators,[162] which are applied to the elastic material of interest to generate the ultrasonic waves. This technology is widely utilized for the inspection of the inner structure of materials and for de-icing large structures such as the blades in wind turbines.[68] The term SAWs refers to sound waves that propagate along the surface of a material, affecting a

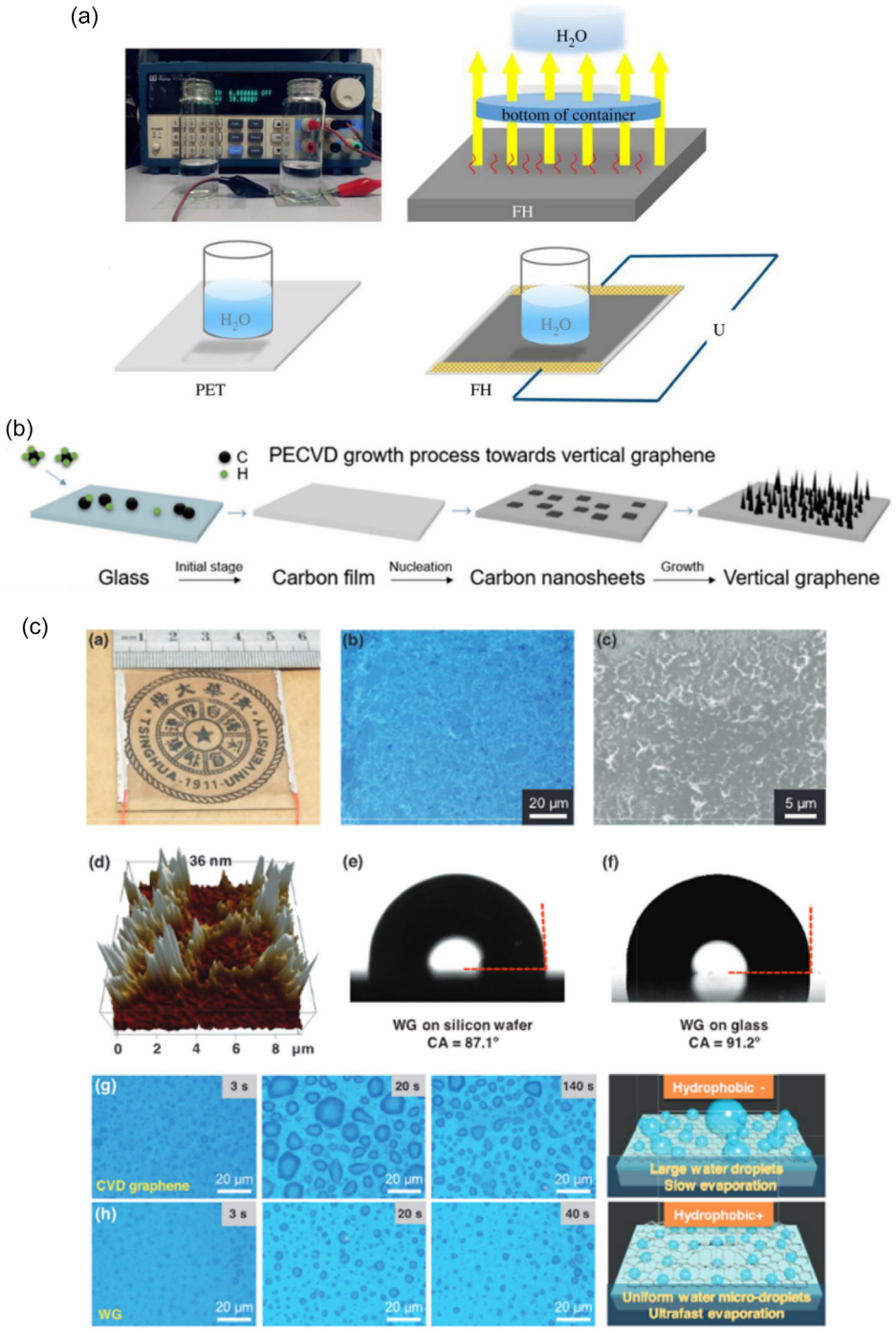

Figure 4. Electrothermal or a combination of both photothermal and electrothermal methods for de-fogging, de-icing, and anti-icing functions. a) Fabrication of CNT-based flexible electrothermal film and representation of heat transfer process involving a pure PET substrate and the submersion of glass in water.[155] b) Fabrication of transparent electrothermal heaters using graphene glass hybrid materials via plasma-enhanced chemical vapor deposition method.[156] c) Illustration of wrinkled graphene (WG)-based anti-icing and de-fogging coating for a glass substrate and their morphologies, as well as the depiction of surface moisture evaporation of both WG and CVD graphene. Reproduced (Adapted) with permission.[157] Copyright 2024, John Wiley & Sons-Books. d) Illustration showing the use of multiresponsive superhydrophobic film with both electrothermal and photothermal functions to demonstrate anti-icing/de-icing performance. Reproduced (Adapted) with permission.[158] Copyright 2024, Elsevier.

depth of ≈1–2 times the wavelength.[163] SAWs are commonly generated through the application of radiofrequency (RF) signals in the MHz and higher ranges to piezoelectric plates or thin films, which are later deposited onto suitable substrates. In its typical configuration, the wavelength of SAW is defined by the characteristics of interdigital transducer (IDT) electrodes, and

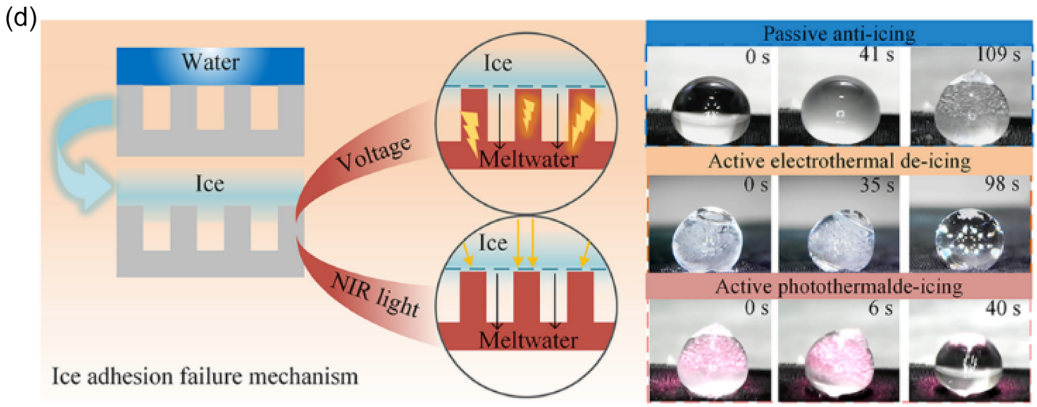

Figure 4. Continued.

the wave propagation takes place with a relatively low attenuation along the piezoelectric layer. This means that a piezoelectric layer must coat the materials or surfaces to be protected against icing. There are also some configurations based on the so-called "superstrate" approach,[164] where low-frequency AWs or SAWs generated in a piezoelectric thin film or system can propagate through the surface of a suitable AW responsive (or with a low-acoustic-impedance) material. Some de-icing industrial systems proposed for large-area de-icing of glass surfaces are fundamentally based on this approach.

Ultrasonic methods commonly use piezoelectric actuators which generate kHz–MHz vibrations, and the shear strains created at the interface by the ultrasonic waves easily cause the ice to fracture and delaminate inducing its removal from the surface. For these ultrasonic devices, various types of waves including guided waves, longitudinal waves, bulk shear waves and Lamb waves are often utilized.[165] For example, feasibility and effectiveness of ultrasonic de-icing using three distinct materials were studied by Daniliuk et al.[68] including $LiNbO_3$, lead magnesium niobate-lead titanate (PMN-PT), and semihard lead zirconate titanate (PZT-4). They reported that the $LiNbO_3$ actuators outperformed PZT ones in terms of environmental concerns and performance.[68] Shen et al.[166] used a circular plate triggered by ultrasonic vibrations at a frequency of 20 kHz to examine the impact of equivalent stress distribution on the de-icing dynamic behavior. They studied the dynamic shedding behavior of frozen droplets under ultrasonic vibration and, based on the characteristics of the ice residue and the uneven distribution of equivalent stress, they have differentiated the de-icing effectiveness and failure zones.[166]

Nevertheless, there are problems with ultrasonic based de-assicing processes, because the unequal/uneven stress distribution and de-icing efficiency are affected by vibration sources' distance.[166] For this reason, the SAW technology would be a better option to succesfully fulfilling de-icing functions as wave propagation occurs throughout the surface of interest, where the waves are evenly distributed. Recent investigations have claimed that SAWs perform better than ultrasonics because the former can integrate multiple functions into a single structure and various substrates as opposed to ultrasonic methods.[131] Moreover, SAWs are energy efficient at surface or interfaces, with distinctive wireless implementation capabilities.

3. Mechanisms of Thin-Film SAWs and Mitigation Principles for Icing on Glass

3.1. Transparent Thin-Film Acoustic Wave Technology on Glass

A transparent ZnO SAW device could be applied on glass as an excellent candidate for simultaneously monitoring fogging and/or icing, as well as for activating de-fogging and de-icing functions.[167] Thin-film SAW devices can work in a continuous feedback way, monitoring fogging and icing-related signals in various cold/hot environments and providing efficient acousto-fluidics and activation functions for de-fogging and de-icing using the same thin-film glass-based SAW platform.[168]

3.1.1. Transparent and Flexible SAW Devices on Glass Substrates

Highly-performant piezoelectric films, such as ZnO, AlN, and PZT, are generally produced on glass substrates using plasma assisted deposition methods, among which magnetron sputtering is widely used because it provides thin films with reasonably good quality. Typically, these films are optically transparent and will not affect the optical and photonic properties of glass substrates. Sputtering preparation techniques are also feasible for other piezoelectric thin-film materials, such as barium titanate ($BaTiO_3$) and $LiNbO_3$, but obtaining high-quality films of these materials presents some difficulties, including complicated optimization processes and high-temperature treatments.[169]

Among the films considered as suitable candidates for SAW actuation, ZnO is one of the most commonly developed piezoelectric thin films because of the benefits it presents. For example, it can be produced straightforwardly with a good crystal quality under mild temperature and vacuum conditions. Film stress is low, and therefore, fabrication of a thick film up to tens of micrometers would be possible. ZnO nanorods and nanostructures compatible with a broad spectrum of AW devices can be also generated.[170,171] Sputtered ZnO thin films on glass usually show dense granular patterns or vertically columnar structures, with thicknesses from hundreds of nanometers up to tens of micrometers. The (0002) plane or the c-axis preferential growth development of the wurtzite ZnO film is required in the crystalline films used for SAW activation. Furthermore, ZnO is

regarded as a biocompatible material with superior physical, electrical, and optical properties.[55,74,172,173] Compared to AlN, it has a larger piezoelectric coupling coefficient, enabling an efficient energy transfer between electrical and mechanical modes.[55,174] Without heating the substrate, a good film crystallinity can be achieved, making the deposition process easier.[175,176] Furthermore, ZnO has good adhesion to most substrates, including glass and polymers, or even cellulose materials,[177] and exhibits minimal film stress depending on deposition conditions.[55,178,179] ZnO can be easily doped for enhancing its piezoelectric properties without losing crystalline or optical quality, as for example in Mn[180] and V[181,182]-doped films. However, there are also some concerns regarding ZnO films' structural, thermal, and chemical stabilities when working under extreme environmental conditions. Although, adhesion problems can be circumvented using plasmas for controlling the interfaces between the ZnO and the selected substrate. Moreover, issues related with chemical wettability and stability, especially under humid or icing environments, can be mitigated by including protecting thin layers.

ZnO films have been used as AW sensors for diverse applications, including monitoring temperature, moisture, pressure, flow, and pH values.[55,56] ZnO SAW sensors can also be used to constantly and wirelessly monitor changes in the mass and density of a medium or other parameters such as conductivity, dielectric response, viscosity, and elastic modulus.[55,56] Methods for determining variations in wave propagation velocities are based on monitoring changes in the resonance frequency, phase angle, or amplitude of reflected or transmitted signals.[55] For instance, ZnO/glass SAW devices with a graphene oxide sensing layer have been used as humidity sensors with excellent sensitivity and quick response.[183] High-sensitivity SAW UV sensors based on piezoelectric ZnO thin films coated on glass substrates have been reported by Wang et al.[6] In addition to this, certain types of SAW modes could be better for ice monitoring, for example, shear components are more sensitive to distinguish water from ice. Lamb wave modes work better in the liquid environment, whereas Rayleigh waves are more effective for de-icing. Karimzadeh et al. also reported the use of a simplified version of IDTs to generate various wave modes for both sensing and actuation.[70]

Besides these sensing applications, many studies utilized ZnO-based SAW devices on glass substrates for acoustofluidics applications. For example, Wang et al. compared the microfluidic performance of ZnO/glass SAW devices with that of ZnO/Si and ZnO/polyimide (PI) SAW systems.[184] They reported that ZnO/glass SAW devices are comparable in performance with that on Si substrates and are advantageous in terms of cost, easy fabrication and compatibility with traditional glass-based biochemical analysis systems.[184] Acoustic streaming has also been achieved using transparent ZnO/glass SAW devices with Rayleigh waves at a high frequency of 154.9 MHz.[5,185]

Although acoustofluidics functions of ZnO/glass SAW devices (such as pumping, jetting, and nebulization) were previously studied, their continuous operation often faces some problems. For example, a poor adherence of piezoelectric films was reported on glass substrates causing peeling-off failure.[186] Furthermore, ZnO/glass SAW devices commonly exhibited a low electromechanical coupling coefficient and AW propagation speed, as compared to those of silicon-based devices.[186] They also incur in significant local heating due to the limited thermal conductivity of glass.[186] Despite these limitations, successfully engineered ZnO/glass SAW devices can be used for a variety of applications, including their usages as active cleaning optical platform to alleviate problems caused by the accumulation of dirt and solid/liquid contaminants on glass lenses, telescope windows, or solar panels, where their implementation can alleviate energy and output losses.[167,187] Apart from ZnO films, many other films, such as AlN, PZT, and $LiNbO_3$ films, have been deposited on glass to leverege different sensing and acoustofluidics functions.[55,188]

Most thin-film-based transparent SAW devices are rigid due to the nature of glass or related transparent substrates.[1,3,4,7] The rigidity of these transparent materials hinders their employment on flexible electronics, despite the substantial impact of flexible devices in curved surfaces of flexible printed circuits, soft robotics, next-generation prosthetics, and personalized and wearable medical systems. Polymers are often transparent and flexible substrates, but regarding applications using SAWs, they present critical issues such as severe dissipation of wave energy and poor thermal stability.[73]

As shown in **Figure 5**a, various SAW devices based on ZnO and AlN thin films on flexible glass have been developed to overcome the restrictions of rigidity. A glass plate thinner than 200 μm is referred to as flexible glass because of its strong bendability and flexibility within this thickness range, comparable to that of substrates made of plastic or metal foils.[73,189] Flexible SAW devices have been used to construct a variety of sensors, such as those intended for humidity[190] and UV detection.[191] They have achieved a strain-detecting range up to $\pm 3000\,\mu s$.[192,193] All the benefits provided by bulk glass are still present in the flexible glass, such as dimensional stability, good resistance to chemical reactions, fair scratch resistance, higher electrical insulation, low-stress birefringence, good temperature tolerance (up to 600 °C, low coefficient of thermal expansion or CTE, $\approx 4 \times 10^{-6}\,°C^{-1}$), good impermeability against oxygen and water, and low root mean square roughness.[73] These properties are superior to those depicted by flexible devices made on polymer substrates.

Numerous application scenarios have demonstrated the tremendous advantages of using ZnO/flexible glass devices. Unfortunately, the instability of ZnO-based SAW devices at high temperatures or harsh environments (such as in alkaline and acidic conditions) or under UV light irradiation limits their use for widespread applications. New solutions are critically needed where ZnO can be effectively protected against the environment without losing its functional and electroacoustic properties. On the other hand, AlN thin films have higher propagation speeds and better mechanical and chemical stability, making them appealing options for high-performance devices in harsh and challenging conditions.[55] For example, Ji et al. fabricated AlN thin-film/flexible glass SAW devices.[194] They investigated fascinating uses, including wearable sensing applications, omnidirectional strain sensing, anti-interference humidity, and UV sensing among others, as shown in Figure 5b.

The electromechanical coupling coefficient (K^2) of AlN thin films is generally low, around 0.5%, which is significantly lower than those of other piezoelectric materials or thin films, severely

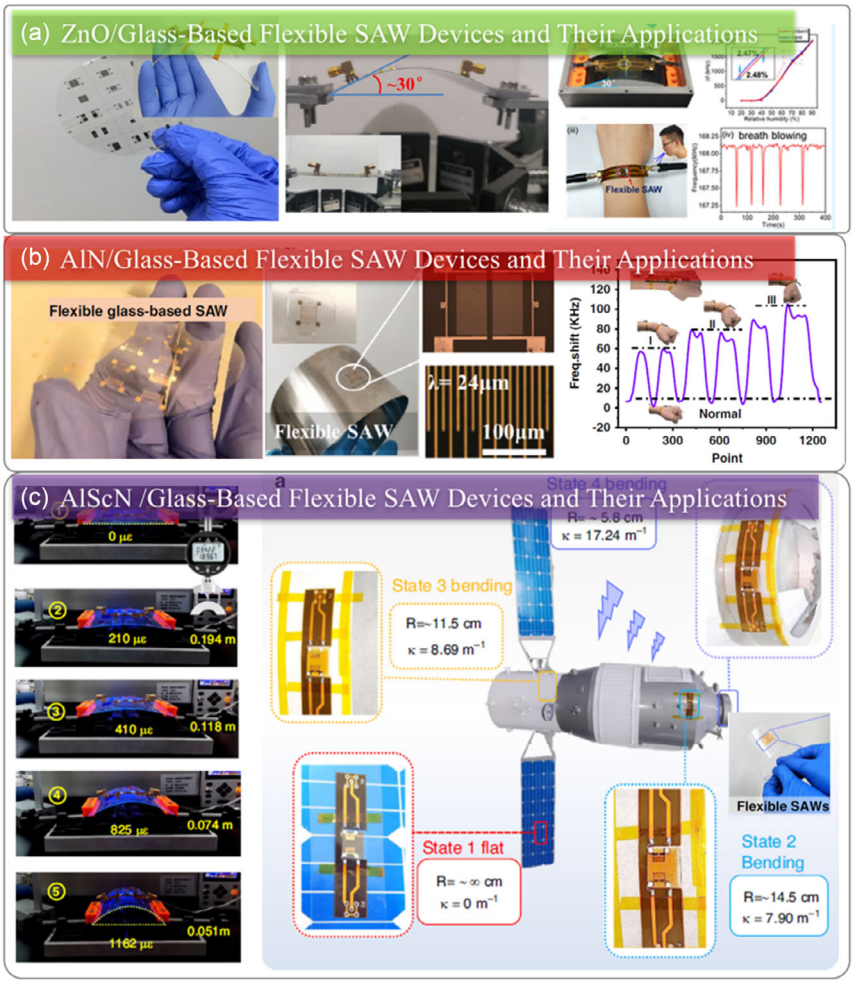

Figure 5. a) ZnO/ultrathin glass-based flexible SAW devices and their sensing applications. b) AlN/ultrathin glass-based flexible SAW devices and their sensing applications. c) AlScN/ultrathin glass-based flexible SAW devices and their sensing applications.[195]

restricting their use for sensing or actuation applications. To address this technical difficulty, researchers have investigated aluminum scandium nitride (AlScN) thin films, in which the piezoelectric capabilities of AlN films can be greatly improved by properly doping scandium (Sc) into the AlN thin films.[195] For example, the ScAlN/flexible glass SAW devices showed an approximately two fold increase in the electromechanical coupling coefficient compared to that of AlN/flexible glass SAW devices. These systems developed a high-precision UV sensing response by integrating machine learning strategies and used it on a spacecraft model to achieve reliable detection on both planar and curved surfaces,[195] as shown in Figure 5c.

Chen et al.[193] reported the fabrication of flexible and transparent ZnO thin-film-based SAW devices using ITO electrodes on ultrathin flexible glass substrates. Metal oxides, such as ITO and FTO, are well-known transparent and conductive thin-film materials. The influence of the annealing process and ITO thickness on the optical properties and AW power transmission properties of these electrodes were investigated in ref. [193]. They were used to make flexible devices such as strain sensors, applying various applied strains up to ±3000 μs with a strain sensitivity of ≈34 Hz $\mu\varepsilon^{-1}$.[193] For high-temperature applications, modified Pt-ITO electrodes[196] have been proposed to cope with the natural instability of ITO under such conditions. Other transparent conducting oxides, such as aluminum-doped ZnO (AZO)[5] or graphene-doped ZnO,[197] have also been proposed for the fabrication of SAW electrodes. A key challenge in this regard is the effective control of the conductive and optical properties of these materials, as required for a stable operation under harsh icing conditions.

At present, considerable progress has been made in the development and sensing applications of bendable or flexible SAW devices. Their unique design and material properties enable their straightforward integration onto various curved surfaces without adding extra volume or weight. This seamless integration capability means that they can be effortlessly applied to existing objects, equipment, or devices without interfering with their original functions or performance. With the ongoing progress in material science and micronanofabrication technology, the performance of these devices can be further enhanced, leading to a broader range of new applications in the future. For instance, in the context of ice monitoring applications, flexible SAW

sensors can be directly attached to aircraft wings, wind turbine blades, or other structures that are susceptible to icing.[72,168] They can also detect changes in surface ice formation, enabling the operation of real-time monitoring and early warning systems. The lightweight and adaptability of these sensors provide an efficient solution for monitoring systems and maintaining structural integrity and functionality.

Jacob et al.[71] demonstrated the efficient migration of de-icing capabilities on the transparent, low thermal conducting substrate materials and proved that SAW-based de-icing was compatible with optical systems. They reported that SAW-based de-icing has the potential to enable industries to efficiently deice large surfaces of transparent and/or low heat-conducting substrates by coating ordinary glass-like materials with transparent, piezoelectric films via standard coating technologies.[71]

3.2. Ice sensing using Thin-Film SAW Devices

As explained above, SAW devices are suitable for highly precision sensing, in addition to providing an efficient mechanical activation. In this section, we will briefly summarize some recent proposals on the application of SAW devices for ice sensing. We will also comment on the possibility of using the same devices for both sensing and activation of the de-icing processes, that is, enabling smart de-icing systems. Most common SAW devices to detect icing processes use a delay line configuration in a piezoelectric substrate or thin film,[50,97,168] with two IDTs facing each other, one acting as emitter and the other as receiver. Both the reflection signals S_{11} and transmission signals of SAWs are commonly measured for ice or fogging sensing purposes.[50,97,168] In general, there are SAW modes that present a higher sensitivity for ice detection, while the others are more recommended for de-icing activation. For example, waves with more shear components are more sensitive to distinguish water from ice, Lamb wave modes are more suitable for liquid environments whereas Rayleigh waves are more effective for de-icing. Activating different wave modes is possible through a specific design of IDTs and electrodes and/or the selection of appropriate electrical signals to excite the piezoelectric films under resonance conditions. There are also recent approaches by which the same types of IDTs can be excited with different electrical signals as to provide either sensing or de-icing capacities to a unique device.

SAW sensors are known for their reliability, sensitivity, and versatility, with intrinsic wireless capacity for real-time monitoring of changes in elastic modulus, viscosity, dielectric, and conductivity properties, as well as mass and density changes.[55,56] As explained, a benefit of thin-film-based SAWs is their ability to combine several functions into one structure on a variety of substrates, including flexible and wearable ones such as silicon, metals, glass, or polymers. For both monitoring and mitigation purposes, this offers one of the best ways to integrate thin-film SAW devices directly onto the surfaces of structural components (such as glass, metal, ceramic, polymer, or composite). Using this approach, thin-film SAW devices can be used as an effective ice or fogging sensor on a large variety of conditions.

Wang et al.[198] reported the use of Lamb waves to monitor the ice formation processes. Since the varying temperature is a remarkable and inevitable factor during ice monitoring, a principle component analysis-based ice monitoring method was proposed to differentiate temperature effects.[198] The proposed method was demonstrated in an icing wind tunnel where the PZT arrays were applied to enhance the guided wave signals.[198] The ultrasonic guide waves combined with a surface treatment were efficient and sensitive for ice monitoring on full-scale wind turbine blades.[198] Schulmeyer et al.[199] utilized a high-frequency SAW dual-mode delay line device on a 64°-rotated Y-cut $LiNbO_3$ substrate and demonstrated both ice detection and temperature measurement. In addition to the shear-horizontal polarized leaky SAWs used by these authors, their findings revealed the exisence of an additional electrically excitable Rayleigh-type wave in the $X + 90°$ direction on the same cut.[199] Both of them can differentiate between liquid water and ice loading and perform temperature measurement as well.[199] IDTs with a large pitch among fingers (i.e., capable of generating long-wavelength AW) deposited on piezoelectric plates or piezoelectric films can be effectively used to generated Lamb-type plate waves.[200,201] Anisinkim et al.[200,201] used a $LiNbO_3$ piezoelectric substrate and IDTs with a large wavelength to generate Lamb-type plate waves, which can be effectively used to detect ice formation from water through monitoring intensity of the transmission signals of a particular vibrational mode.

The possibility of using the same piezoelectric device for both sensing the formation of ice and activating the de-icing has been recently addressed.[69,70] One common approach consisted of using a piezoelectric plate excited with a pair of flat electrodes in a lateral field configuration. The thickness shear mode (TSM) AWs generated at lower frequency (3–4 MHz) excitation conditions provided a good sensitivity for the detection of icing phenomena. In addition, narrow S_{11} peaks at its resonance (i.e., high Q factors) resulted in good sensitivities for both temperature changes and ice formation. Karimzadeh et al.[70] showed that a piezoelectric plate device with a delay line configuration using IDTs may generate TSM waves, providing the possibility for monitoring icing phenomena with a high sensitivity, whereas de-icing was possible applying a higher electrical power to generate SAW Rayleigh waves at the resonant frequency of the device.[70] Such a hybrid function was achieved by changing the polarity of the two combs of fingers integrated in the IDTs with an external electrical switch. In the TSM mode, the two combs were polarized at the same voltage with one IDT at ground potential, whereas in the normal SAW mode, one of the electrodes combs in each IDT was polarized at ground and the other at the operating voltage. Switching from one mode to the other enabled the detection of ice using the very sensitive TSM mode and then the ice removal using SAW activation.[70]

Zeng et al.[168] reported that the changes in the propagation velocities of the SAWs (which induced changes in the resonant frequency or frequency shifts of the SAW device) could be affected by multiple factors including temperature changes, electrical effects, and mass loading.[168] **Figure 6** shows that in a cold environment above the freezing temperature of water, water molecules are usually absorbed on the surface of the SAW device, especially at high humidity. This mainly causes a mass loading effect.[168] Meanwhile, other effects are also in play, such as changes in the impedance, conductivity, and capacitance of the SAW devices.[168] Figure 6 illustrates all of these changes,

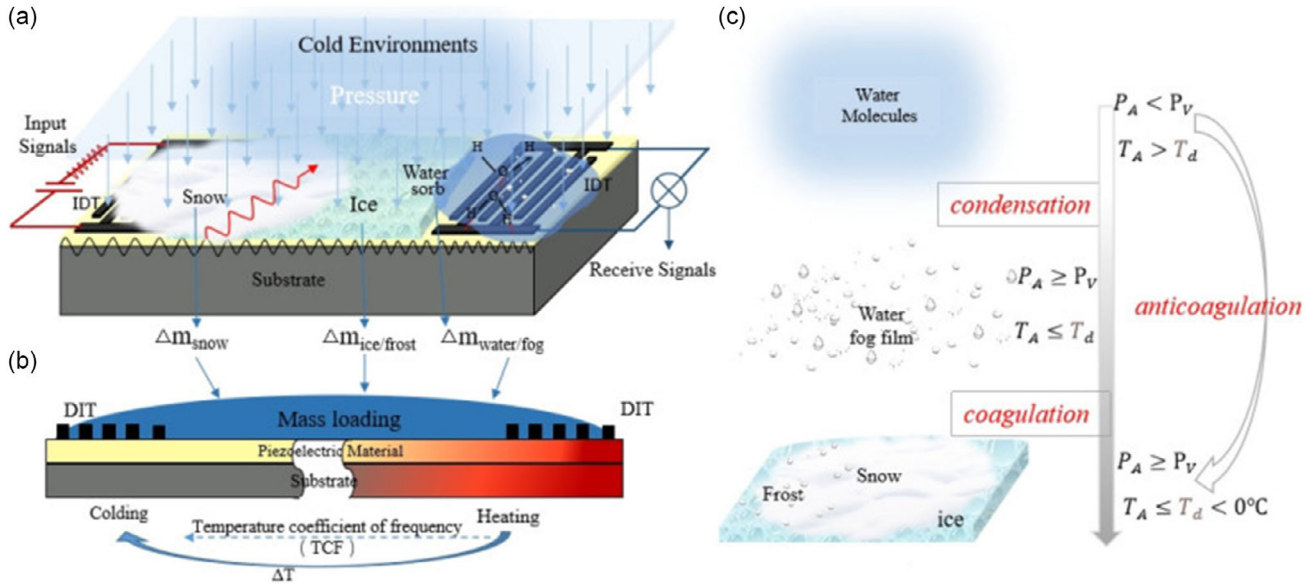

Figure 6. Illustration on the effects of the environmental conditions on a SAW device. a) Water molecules, fog film, snow, and ice formed on SAW surface; b) mass loading and temperature effects from water molecules, fog film, snow, and ice formation on SAW device surface; c) process by which changes in the temperature and vapor pressure affect the water vapor to form fog and frost.[168]

which affect the resonant frequencies of the SAW device differently.[168]

4. Progress of Thin-film SAW on Glass for Active De-icing and Anti-Icing

Different physical interactions intervene during the SAW activation of substrates, leading to the removal of ice or the prevention of the ice accretion process. This section summarizes the advances made in the understanding of these effects, with special insight into the case of SAW actuation on glass substrates. The specificities of these interactions when dealing with rime or glaze ice are also summarized in addition to recent advances in the use of superstrate approaches to cope with the de-icing and cleaning of large surfaces of glass using SAW.

4.1. SAW Mechanisms for De-icing and Anti-Icing

Thin-film SAWs have great potential as an emerging ice mitigation strategy, due to their high energy efficiency and effective integration onto structural surfaces such as glass.[67,131] Thin-film SAW devices on glass can be used for both anti-icing and de-icing applications due to their ability to generate waves and other related effects such as acoustothermal effect, acoustic radiation force, and acoustic streaming. However, anti-icing/de-icing processes activated by SAWs involve complex interfacial evolution and phase changes. Thus, it is critical to understand the nature of dynamic solid–liquid–vapor phase changes and ice nucleation, growth and melting events under SAW agitation.[131] As illustrated in **Figure 7** for the particular case of rime ice, both ice accretion and de-icing processes are strongly linked with dynamically interfacial structure changes induced by SAW

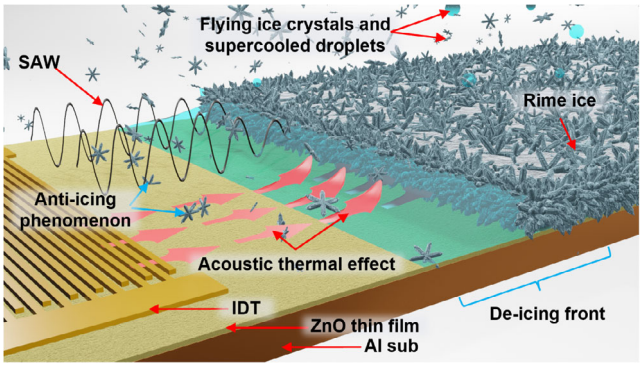

Figure 7. An illustration of principles for SAW propagation in three different configurations with the presence of (1) solid and dry porous ice, (2) the ice/liquid mixture where some of the ice is partially melted, and (3) the liquid water/water vapor stage where water has been changed into liquid form and then gradually evaporated.[67]

activation, together with acoustothermally induced localized heating, which facilitates the rapid melting of ice crystals.[67,131] The interactions of SAWs with a thin water layer formed at the ice/substrate interface have been reported to result in significant streaming effects, which lead to further damage and melting of ice, liquid pumping jetting, or even nebulization (see Figure 7).[67,131]

This section will summarize the physical principles involved in various research methodologies that utilize thin-film SAW on glass to promote both anti-icing and de-icing functions.

4.1.1. Nanoscale Earthquake-Like Interfacial Vibrations

Nanoscale vibration (which are induced by the propagating SAWs from the surface into ice or liquid water) is one of the

main mechanisms for ice removal using SAW devices.[65,131] The nanoscale "earthquake" effects that SAWs generate on the device surface after the formation of the ice nuclei result in considerable surface vibrations, which reduce the ice nuclei adherence to the surface.[65] As a result, SAWs play a key role in the anti-/de-icing process by preventing ice accumulation and effectively removing the formed ice.[131] Ice bonds are weakened because SAWs' nanoscale vibration weakens the van der Waals forces.[65] During the freezing process, tiny ice fractures, also known as the formation of air voids, frequently occur at the ice–structure interface.[65] The nanoscale "earthquake" produced by the SAWs can efficiently accelerate the propagation of these cracks.[65] Because of the strong vibrations at the interface, further cracks may also be induced in the bulk of ice.[65]

There is, however, little information about the way by which the SAWs transmit their mechanical energy into the ice and how this process depends on the type of wave used in each case. Recently, Pandey et al.[202] studied the dependence of the de-icing efficiency of glaze and mixed types of ice on the AW modes, using either Rayleigh SAW or Lamb waves. It was realized that on a $LiNbO_3$ chip, de-icing using long-wavelength Lamb waves was energetically more efficient than using the Rayleigh SAWs.[202] **Figure 8** shows finite-element simulations of the mechanical energy transmitted from the activated substrate to an ice agglomerate when using Rayleigh SAW or Lamb waves (Figure 8a,b).[201] Results revealed that while the Rayleigh SAWs are efficiently damped by the ice in a relatively shorter interface length (i.e., SAW mechanical energy is efficiently transmitted to the ice within a length of about ten wavelengths (Figure 8c), the larger-wavelength Lamb waves transmit less efficiently their mechanical energy to the ice aggregate but can propagate without complete attenuation through a much larger ice–substrate interface zone (Figure 8d). Paradoxically, it appears that efficient transmission of mechanical energy into the ice structures does not necessarily mean a higher de-icing efficiency.

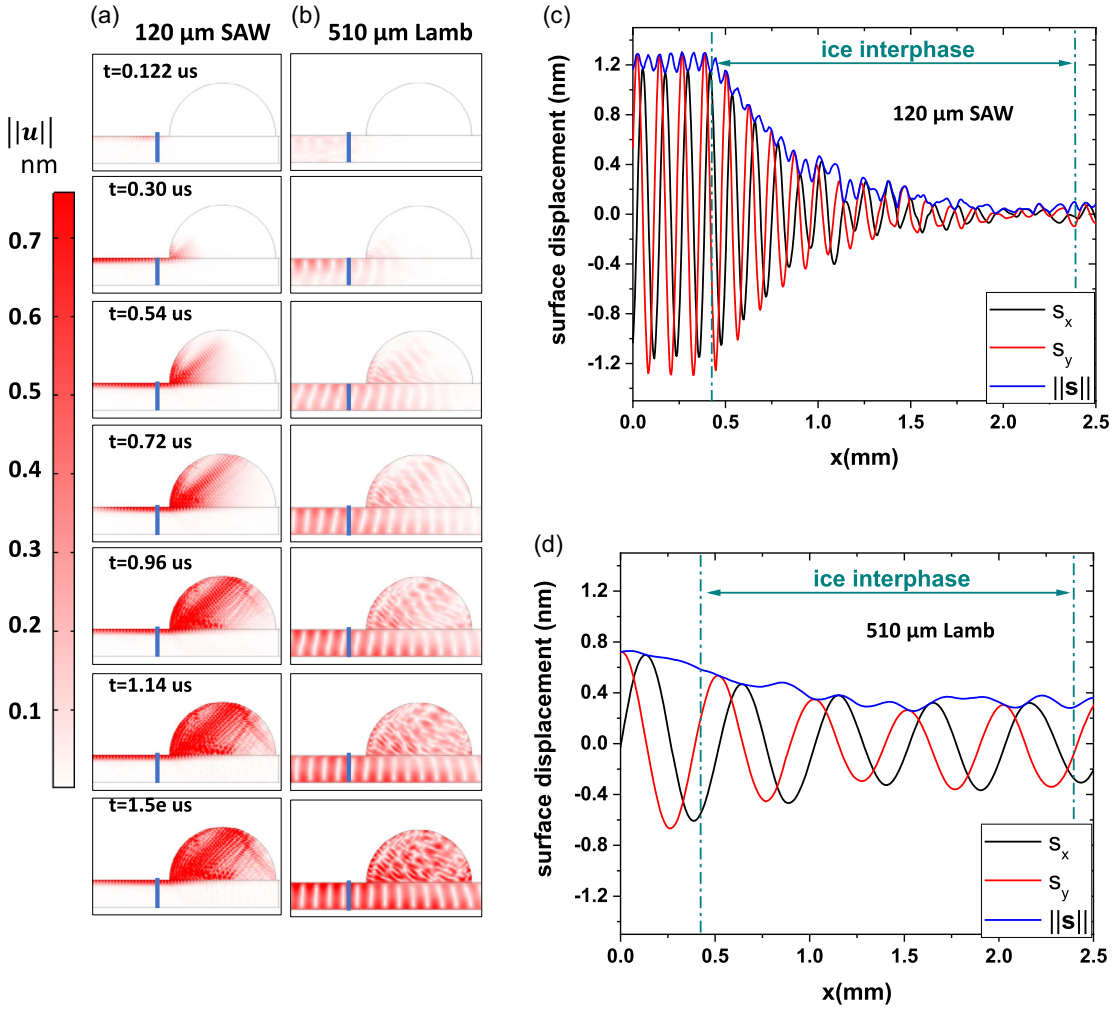

Figure 8. AW–ice interactions and surface displacements comparing SAWs and Lamb waves. Time-dependent simulated snapshots in the form of intensity color maps of the AW-induced displacements in the lithium niobate (LN) chips with an ice aggregate on their surface. The vertical line along the plate signals the location of the last finger of the simulated IDT. a,b) Calculations for the 120 µm SAW and 510 µm Lamb wave, correspondingly. c,d) Surface displacements at the surface of LN substrate as a function of wave propagation along the × coordinate direction for the (c) 120 µm SAW and (d) 510 µm Lamb wave interacting with the ice aggregate on the surface.[202]

A de-icing mechanism was proposed to describe the effect of Lamb waves. It involves a first stage consisting of the cracking activation along a larger ice–interface zone, followed by a progressive vertical melting of ice, beginning at the interface to finally affect the whole volume of ice.[202] This mechanism differs from that proposed for a Rayleigh SAW,[71] which involves the lateral progression of a water–ice front and the consequent heat transmission at the water–ice interface (see Section 4.1.3). Heat losses from water into the air and poor lateral heat transmission from water to ice (this latter is a good thermal insulator) would be key factors hindering a rapid progression of ice melting in this case, therefore negatively affecting the power efficiency of the process when using Rayleigh SAW.[71]

4.1.2. Streaming and Radiation Effects into the Liquid

After the first melting of ice takes place at the interface, a mixture of liquid water and small ice aggregates or nuclei will coexist in this zone. A similar situation is expected at the initial stages of a freezing process. The primary force that the SAW applies to a single particle in a fluid is described by the acoustic radiation pressure (F^{ARF}).[61] Meanwhile, interactions among various particles that are fluidly bound produce secondary acoustic radiation pressure effects. Depending on their mechanical properties, the particles are driven toward either pressure nodes or antinodes by both the primary and secondary acoustic radiation forces.[61] The acoustic radiation force (F^{ARF}) is determined by taking the surface integral of the time-averaged second-order pressure p_2 and momentum flux tensor $p_0 v_1 v_1$ at a fixed surface immediately outside the oscillating sphere.[61] A generic solution for this force has the following expression[61]

$$F^{\mathrm{ARF}} = -\int_{\partial\Omega} da\{\langle p_2\rangle \mathbf{n} + p_0\langle(\mathbf{n}\times v_1)v_1\rangle\} \tag{1}$$

where $\mathbf{n}$ denotes the unit normal vector of the particle surface directed into the fluid. In general, the particles in a fluid are subject to the net acoustic radiation force and the SAW acoustic streaming-induced Stokes drag force F^{drag}.[61] The final effect is influenced by particle size. Particles larger than a given threshold size will be subjected to motion control by the acoustic radiation force. A few factors that affect the size requirement include the kinematic viscosity, acoustic contrast factor, and actuation frequency.[61] Particle size, shape and structures, fluid viscosity, and the fluid flow field all affect the Stokes drag force, or F^{drag}. For a spherical particle of radius r, medium viscosity η, and relative velocity v, the drag force, F^{drag} is given by the following equation[61]

$$F^{\mathrm{drag}} = 6\pi\eta r v \tag{2}$$

As such, acoustic radiation force (F^{ARF}) and acoustic streaming drag force (F^{drag}) are the two forces applied to solid particles, i.e., to the ice nuclei suspended in the liquid when the wave energy is dissipates into it.[65] A dimensionless coefficient (k) was applied to assess the dominating force in different liquids containing different types of particles.[65] Particles in the fluid are driven by a net acoustic radiation force if $k \geq 1$.[65] When k is less than 1, the system is dominated by acoustic streaming,[65] and dissipation of SAW energy into the liquid causes liquid flow or microstreaming, resulting in the ice nucleolus and liquid to move relative to one another.[65] The SAW frequency (or wavelength) and applied RF powers of SAWs affect this flow.[65]

In brief, due to the acoustic field's scattering effects, particles such as ice nuclei exposed to an AW field are under the action of both direct and indirect irradiation forces.[61] The dominant force that the SAW applies to a single ice particle in a fluid is described by the primary acoustic radiation pressure (F^{ARF}).[61] Meanwhile, interactions of sound waves with other particles that are fluidly bound produce secondary acoustic radiation pressure.[61] The SAW acoustic streaming effect will induce Stokes drag force F^{drag}, causing the ice nuclei to flow with the liquid. All these effects will affect the nuclei's behavior during icing processes.

4.1.3. Localized Heating Effects

During SAW agitation and propagation, the temperature of the solid surface and its surrounding liquid is increased as a result of the localized thermal energy generation at the ice/substrate interfaces caused by the acoustothermal effect (SAW radiation, energy dissipation, and related Joule thermal effect).[65,158] Although there could be heating effects due to electrical losses in the IDTs, melting is dominantly driven by the acoustothermal effects of SAWs through ice/water interactions.[158] These will be of different nature depending on whether we deal with anti-icing or de-icing. During the anti-icing (or anti-freezing) process, the ice nucleus's expansion is restricted by the acoustothermal effect, which will reduce the interfacial bonding capacity to the solid cold surface.[65] Moreover, after ice accretion, the acoustothermal effect will considerably reduce the ice adhesion force and cause the interfacial ice layer to melt, resulting in an effective de-icing effect.[65,155] The SAW devices will also be heated up as the temperature increases, which will cause the water droplet to interact more effectively with impurities on the surface and drive them away more effectively during liquid transportation.[167]

4.2. Rime Versus Glaze Ice De-icing and Anti-Icing Using Thin-Film SAWs

Due to their different mechanical properties, glaze and rime ice are expected to behave differently when exposed to SAW activation. Hence, differences may appear always that the previously outlined physical processes affect differently the de-icing of these two types of ice. Similarly, variances can be expected depending on the water repellence of the surface (i.e., the hydrophobicity or slippery degree). It is noteworthy that a challenging topic in this regard is the modification of surface states of the piezoelectric films to bestow them specific icephobic functionalities, while simultaneously protecting them against environmental degradation. However, the strategy of coating the piezoelectric film with other materials requires a precise analysis of the acoustic impedance and compatibility with SAWs (i.e., the capacity to efficiently transmit the SAWs with little or no attenuation). Adjustment of the thickness is also critical in this regard. Anyhow, it is noteworthy that the incorporation of an anti-icing coating will provide aging and environmental protection to the whole device, including piezoelectric layer and IDTs. This would ensure long-term

reproducibility and stability for outdoor applications, particularly under extreme conditions such as the marine environments.

Using glaze ice as a case example, the scheme in **Figure 9** shows that SAWs can be utilized to accomplish both anti-icing and de-icing tasks.[65,131,158,203] In addition, it shows that a functional layer can be deposited onto the ZnO film to enhance the surface hydrophobicity.[65,203] When a water droplet is placed onto this ZnO thin film at a certain freezing temperature, the surface hydrophobicity results in a hybrid Wenzel and Cassie–Baxter state as shown in Figure 9a.[65] The nano- and microscale structured ZnO surface of the icephobic coating can effectively delay and slow down the ice formation, although ice nucleation and growth will still occur once the thermodynamic equilibrium is reached at the water/structure contact point.[65] The icesubstrate contact of a large ice block layer has four types of interfacial forces operating at the ice–cold interface, that is, Van der Waals forces, electrostatic forces, hydrogen bonding, and mechanical adhesions.[65] SAWs create nanoscale vibrations comparable in scale to the van der Waals forces that can weaken the bonds between ice molecules.[65]

Figure 9b shows that nanoscale "earthquake" effect, including the effect of acoustic radiation force, acoustic streaming, and acoustic thermal effect on ice nucleation and development.[65] Van der Waals forces are one of the principal adhesive forces between the ice nuclei and the solid surface.[65] As an ice nucleolus forms, the device's surface vibrates significantly under the SAW agitation,[65,204] and as a result, any ice nucleolus that is formed and developed on the surface becomes less adherent and easily detached. The temperature of the solid surface and the surrounding liquid is effectively increased due to the simultaneous release of localized acoustothermal energy at the ice/structure interface, as shown in Figure 9b.[65,204] When

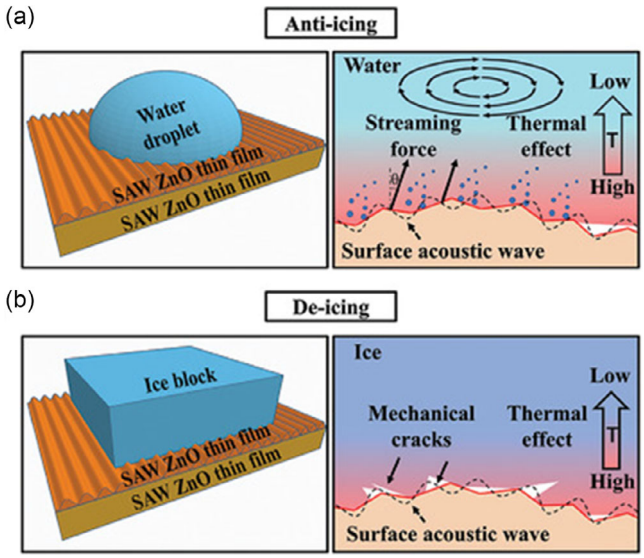

Figure 9. Illustration of a) 3D model of a hydrophobic SAW device with no power applied, and zoom of the ice nucleation at the water–substrate interface. b) 3D model of a hydrophobic SAW device with power applied to induce an anti-icing function and zoom of the SAW anti-icing process. Reproduced (Adapted) with permission.[65] Copyright 2024, John Wiley & Sons-Books.

the SAWs propagate into the liquid, the ice nucleolus becomes detached within the liquid and is largely driven by acoustic streaming. The resulting microstreaming or flow can lead to a relative displacment of the ice nucleolus in the liquid medium.[65] In this way, the nanoscale vibrations and the acoustothermal effect many induce that the generated ice nuclei can freely flow alongside the liquid's streaming,[65] thus improving the anti-icing effect through the limitation and slowing down the rapid formation of ice nuclei.[65]

Ong et al.[72] using ZnO/glass SAW devices as a mean to fulfil both anti-icing and de-icing functions reported the glaze ice de-icing as shown in **Figure 10**a. Droplet freezing was followed on a ZnO/glass SAW device in the absence of SAW energy. Ice was formed after ≈19 s, and the progression of a freezing front could be observed, while the unfrozen portion remained spherical, as shown in Figure 10b,c. After about 80.9 s, the ice began to push up on the droplet, resulting in a pointed tip. On a surface treated with the hydrophobic polymer CYTOP but without SAW power, glaze icing begun after around 42.3 s. Ice crystals were only formed after ≈109 s. Compared to untreated devices, the hydrophobically treated CYTOP layer delayed droplet freezing, as shown in Figure 10b.

Figure 10d shows the timeframes for droplets turning into ice at different RF powers, with and without SAW agitation. When no RF power was applied, the freezing times were comparable on treated and untreated surfaces. At a considerably lower power of 0.21 W, the surface vibrations under SAW agitation inhibited the formation of supercooled droplets. However, at a power of 0.37 W or higher, the freezing time increased significantly, demonstrating an effective anti-icing behavior. No frozen droplet phenomena were observed at RF powers of 0.62 and 0.81 W within the 600 s timeframe.

The de-icing results using ZnO/glass SAW devices with an RF power of 1.41 W are shown in Figure 10e. The SAW's acoustothermal effect at the ice/glass interface and the induced localized vibrations caused changes in the ice structure. Fracture was found at the solid/ice interfaces during the de-icing process, spreading and degrading the ice's adhesion to the glass. The localized acoustothermal effect eventually produced the melting of the ice, turning it into liquid. When the SAW power was applied, the transparent glaze ice with CYTOP showed similar phenomena, as seen in Figure 10d. Adding CYTOP reduced de-icing time, as shown in Figure 10f. Figure 10g summarizes the timeframes for droplet de-icing, clearly decreasing with increased RF powers.

Nampoothiri et al.[205] studied the dynamics of de-icing of microliter volume water droplets (1–30 μL) exposed to low-power (0.3 W) SAW actuation generated by in a system formed by an IDT on $LiNbO_3$ substrate and compared these results with those on glass substrates. The time variation of the volume of liquid water from the onset of SAW actuation to complete de-icing took 2.5–35 s depending on the droplet volume.[205] They reported that the de-icing phenomenon could be mainly attributed to acoustothermal heating, which was found to be greatly influenced by the loss of ice adhesion with the substrate and the acoustic streaming within the liquid water.[205] Acoustothermal heating inside the droplet was demonstrated by the analysis of the temperature distribution inside the droplet obtained using infrared thermography. Acoustic streaming was observed upon the detachment of

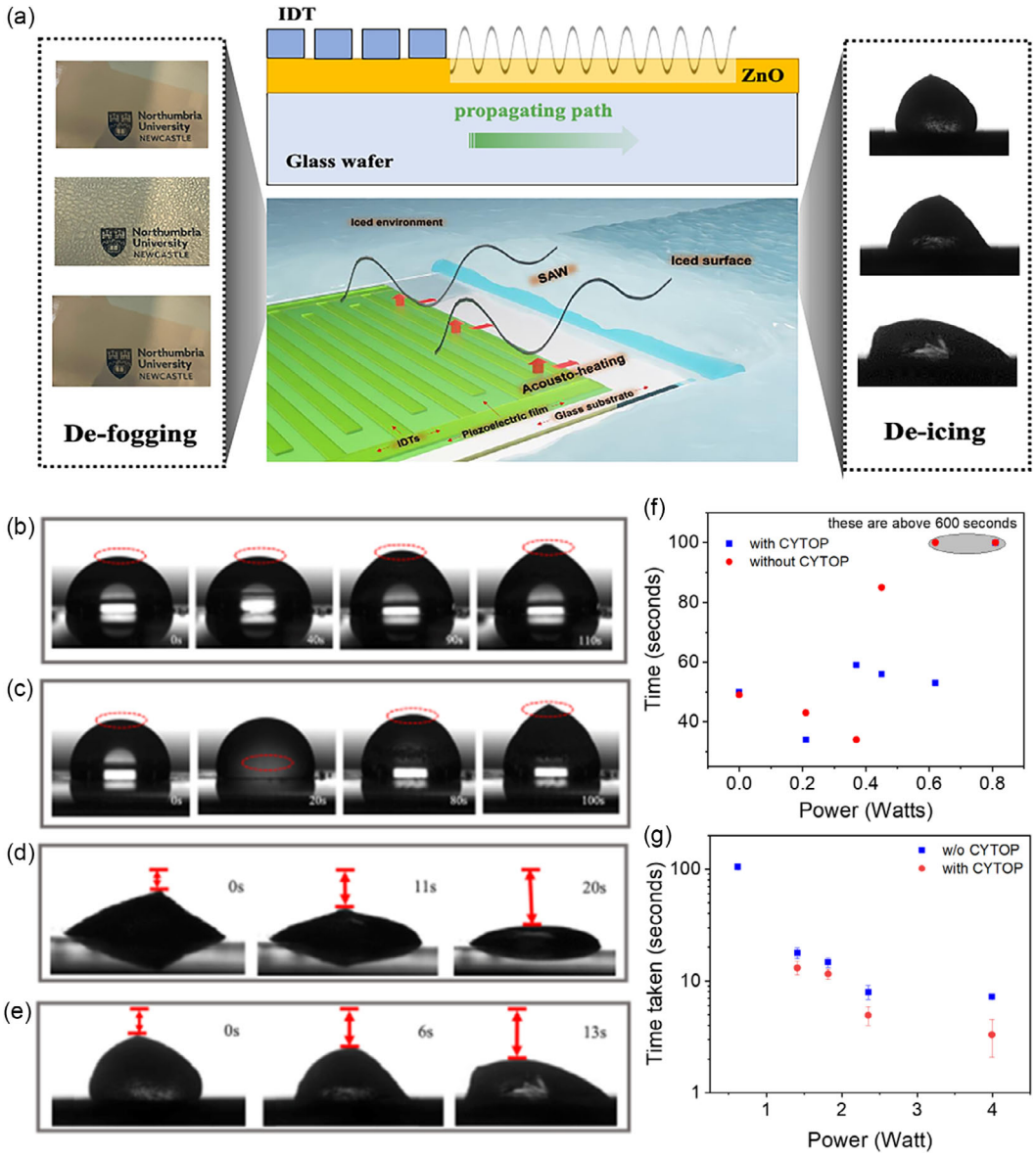

Figure 10. a) Illustration of the use of a ZnO/glass SAW device to promote both de-fogging and de-icing functions. b–c)Freezing of a droplet on a ZnO/glass SAW device at different RF powers, comparison of b) untreated surfaces and c) CYTOP-treated surfaces. d) De-icing on ZnO/glass SAW device without CYTOP at 1.41 W; e) with CYTOP treatment at a power of 1.41 W. f) Time required for a droplet to become ice on the ZnO/glass SAW device at various RF powers. g) Time taken for droplet de-icing at various RF powers. Reproduced (Adapted) with permission.[72] Copyright 2024, Elsevier.

ice from the substrate.[205] The de-icing time was found to increase linearly with droplet volume, as experimentally observe and further verified using a theoretical model.[205]

Addressing the problem of de-icing large area surfaces of transparent glass, Jacob et al.[71] studied the de-icing functionality with both a self-supported piezoelectric material ($LiNbO_3$) and a ZnO piezoelectric thin film deposited on FS. The latter system proved the compatibility of SAW methods with materials of practical relevance. Its applicability to large and transparent substrates was demonstrated by placing the IDTs required for activation close to the edge of the substrate, leaving most of the surface unaltered.[71] The de-icing mechanism of glaze ice by SAW activation was revealed simulating the SAW propagation on ice-covered surfaces and by the experimental analysis of the ice melting process. The schematic illustrations shown in **Figure 11**a–d show the de-icing mechanism taking place when applying Rayleigh SAW to de-ice large-area substrates and the finite element model (FEM) results of the SAW propagation along the ice–substrate interface.[71] The de-icing mechanism involves a combination of ice mechanical stress activation taking place at the beginning of the process, followed by streaming and heating through the initially formed water/ice front, as shown by the thermographic images in Figure 11e–g.[71] With this experiment, Jacob et al.[71] proved that possible Joule effects due to

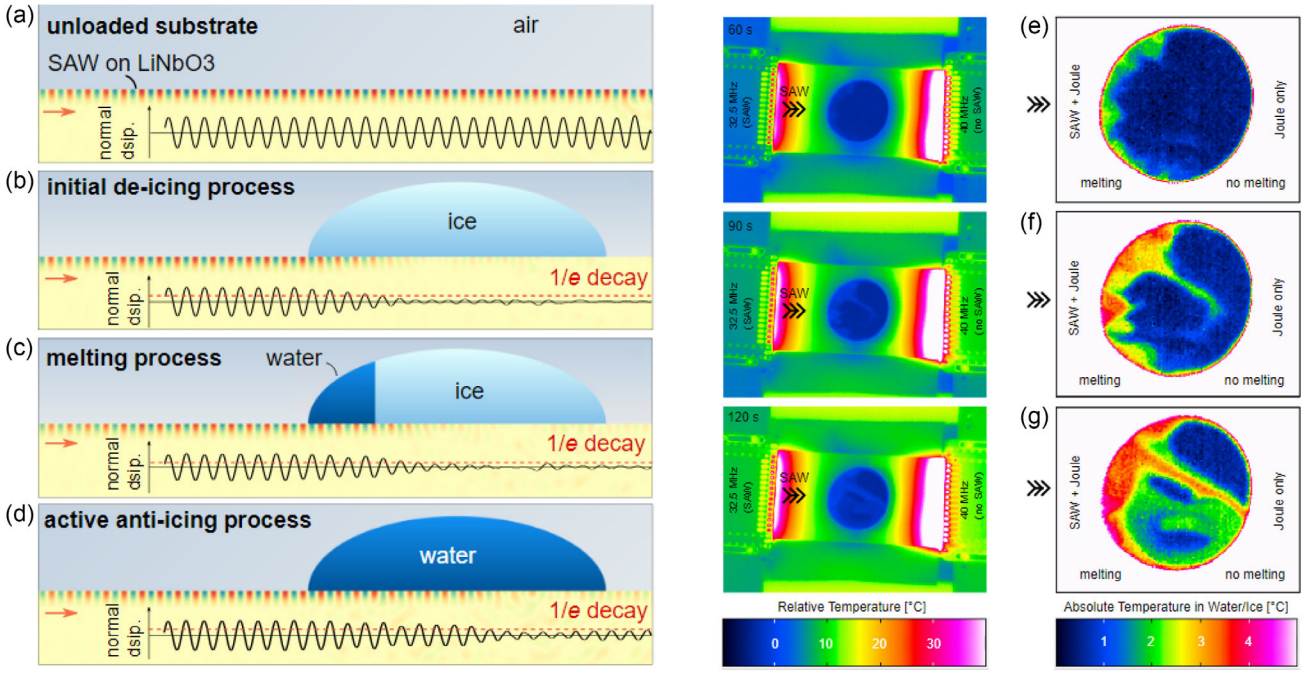

Figure 11. Schematic of de-icing of large substrates and FEM model calculations of SAW interaction with water and glaze ice for the different de-icing process stages and thermographic camera monitoring of the de-icing process. a) Reference model without water/ice. b) Pure ice, indicating a small SAW interaction zone (5λ), c) water and ice, indicating an extended interaction zone (7λ), d) pure water, indicating a large interaction zone (10λ). e–g) Thermographic camera monitoring of the de-icing process upon activation of the IDT at (left IDT) and out (right IDT) of resonance conditions. Note that maximum temperature is recorded for the IDT at the right side due to Ohmic losses, while the streaming and progression of melting occurs from left to right in the big ice aggregate despite that the temperature at the IDT at the left side is much smaller. Reproduced (Adapted) with permission.[71] Copyright 2024, John Wiley & Sons - Books.

Ohmic losses in the IDTs could be disregarded, a conclusion which was reached upon monitoring the local temperature variations detected in the thermographic images during SAW activation at and out of resonance conditions (Figure 11e–g).

Figure 12a–f illustrates the de-icing process of rime ice on a 28.12 MHz ZnO/glass SAW device treated with CYTOP. The initial rime ice was solid/porous and loosely attached (Figure 12a). Mechanical vibrations from the SAW acoustic energy caused damage to the ice clusters (Figure 12b), leading to its removal in certain regions (Figure 12c). SAW energy also resulted in interfacial localized heating on the ZnO thin film (Figure 12d), causing the porous ice to shrink (Figure 12e). Ultimately, the de-In icing process was completed through SAW agitations and acoustothermal effect (Figure 12f).

In a recent work it is shown that phase changes occur along with increased SAW agitation, beginning in the vicinity of the top region around the IDT area.[131] Due to the combined impacts of thermal heating and AWs, an icing front made of a liquid/ice mixture forms and moves swiftly in the SAW direction. As the de-icing process continues, the breadth of the de-icing front is clearly increased (from **Figure 13**a–c). As shown in Figure 13d, the de-icing front can be divided into four areas, that is, the liquid area, the liquid-rich (with ice) area, the ice-rich (with liquid) area, and the rime ice area. Because of the low acoustic impedance in liquid and liquid-rich locations, the SAW wave energy is rapidly absorbed, resulting in notable internal streaming and phenomena such as liquid transportation, jetting, or nebulization.[131] The acoustic streaming drag force and acoustic radiation force cause little ice crystals to flow throughout the liquid. AW energy is rapidly dispersed into the liquid in the liquid-rich and ice-rich regions, leading to strong streaming and localized heating effects. The de-icing process is then accelerated by the improved mass and heat exchange caused by acoustic streaming. A number of things happen in the rime ice area, such as ice crystals or clusters breaking apart and collapsing in the area where the substrate and rime ice meet at the interface.[131]

In summary, as reported by Yang et al.[131] the primary de-icing processes are the phase transitions brought about by the combination of the thermal and acoustic agitation effects. Ice crystals or clusters break apart and collapse as a result of the surface vibrations caused by the AWs' effect on the interfacial structures between the rime ice and the SAW device interface. The ice/device contact experiences phase transition as a result of the thermal effect building up, and the melted liquid and ice crystals swiftly fuse together. In addition to the two main mentioned mechanism, the inner flow and streaming force greatly increase the mass and heat exchange, which effectively accelerates the de-icing process, as the SAW waves propagate into this ice–liquid combination front.[131]

Moreover, de-icing functions can be fulfilled via wireless technologies. During the integration of wireless technologies with SAWs, a wireless power transfer (WPT) system was designed to match the resonant frequency of the SAW device to ensure optimal performance at its operating frequency. Ong et al.[206]

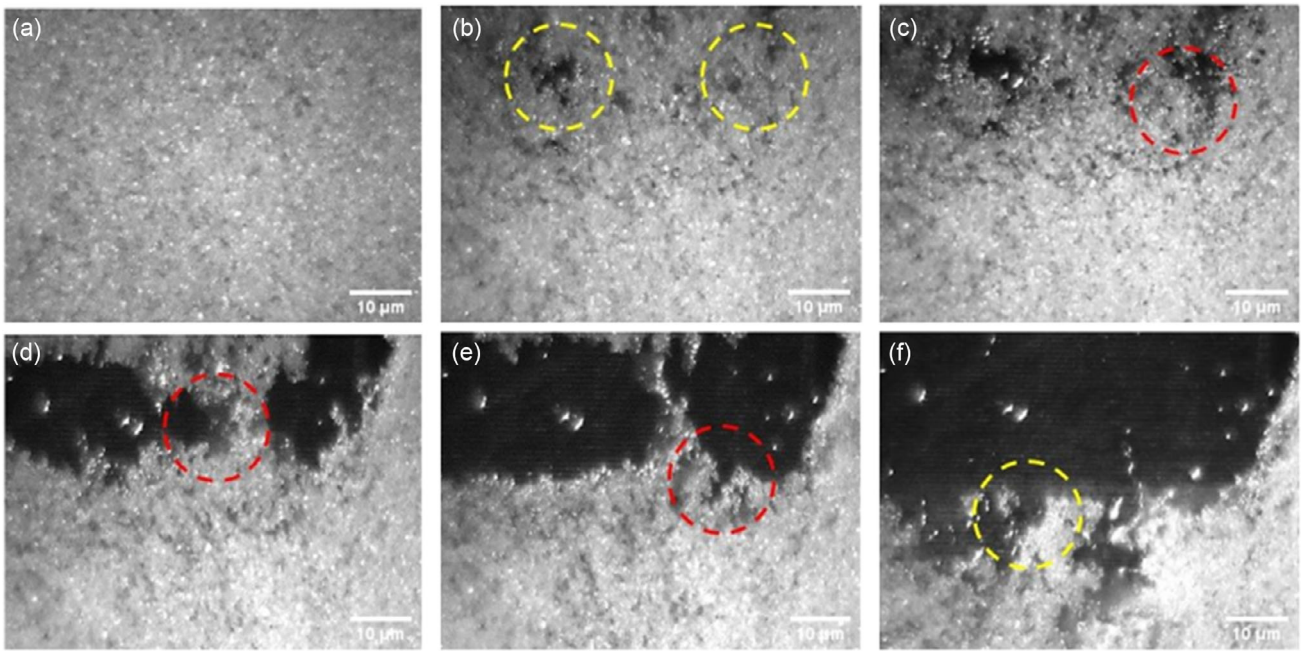

Figure 12. The 28.12 MHz ZnO/glass SAW device that was treated with CYTOP for the purpose of rime ice de-icing was observed at a) 0 s, b) 5.912 s, c) 6.868 s, d) 8.420 s, e) 10.988 s, f) 34.040 s using a scale bar of 10 µm. Reproduced (Adapted) with permission.[72] Copyright 2024, Elsevier.

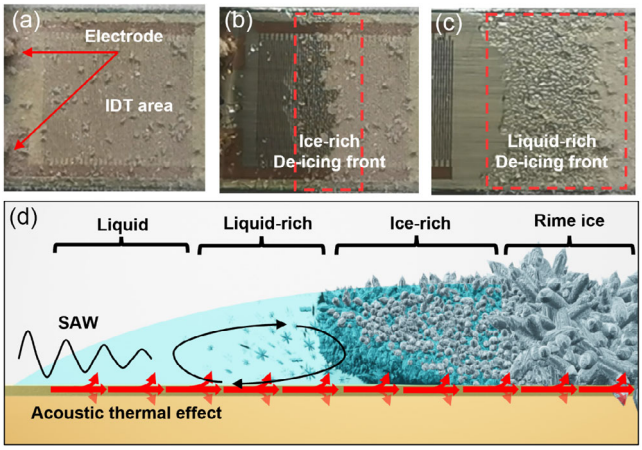

Figure 13. a) Depiction of the surface morphology of the iced SAW device (top view in the IDT area). b) Depiction of the area with an ice-rich de-icing front. c) Depiction of the area with a liquid-rich de-icing front. d) An illustration of the de-icing front with four different regions.[131]

presented an integrated thin-film SAW and WPT system on glass substrates to fulfil both de-fogging and de-icing functions. They demonstrated that through the integration of a WPT system, the localized heating effects and thermal generation induced during de-icing and de-fogging were dramatically reduced.

4.3. Thin-Film SAW De-icing of Large Glass Surfaces Using a Superstrate Approach

In a classical configuration, de-icing a glass surface by SAWs would require coating the glass surface with a thin piezoelectric film and the integration of IDT electrodes onto the films. This configuration faces the challenge of homogeneously depositing the piezoelectric film over the whole glass surface area. At the industrial level, alternatives have been proposed based on superstrate approaches and AW frequencies around 1 MHz. In a patent, Trevett et al.[207] claimed the cleaning, water removal, and de-icing of laminate windshields. The procedure consists of the distribution around the windshield of AW generators with large, interdigitated electrodes. The generated waves propagate through the external glass laminate and induce de-icing. Another recent patent[208] proposed a similar superstrate approach introducing the possibility of using stickable superstrate layers made of PMMA (polymethyl methacrylate) films. In this patent, transparent films with incorporated piezoelectric layers and IDTs are stacked on the surface of glass (or any other material) and serve as propagating medium of the AW excitation. The possibility of replacing this plastic cover is an obvious advantage in case the glass support has to be preserved. The proposals in these patents open interesting fields of research to optimize the different variables of the developed procedures and increase the power efficiency of the systems.

5. Thin-Film SAWs for De-fogging Applications

Successfully fabricated ZnO/glass SAW devices can be used for wide-range applications through their incorporation as an active surface cleaning platform to alleviate the problems due to the accumulation of dirt, solid/liquid contaminants, ice, frost, and fog on glass lenses, telescope windows, or solar panels that can result in losses in energy and outputs.[187] Similar to the case of icing protection, the mechanical vibrations induced by SAWs

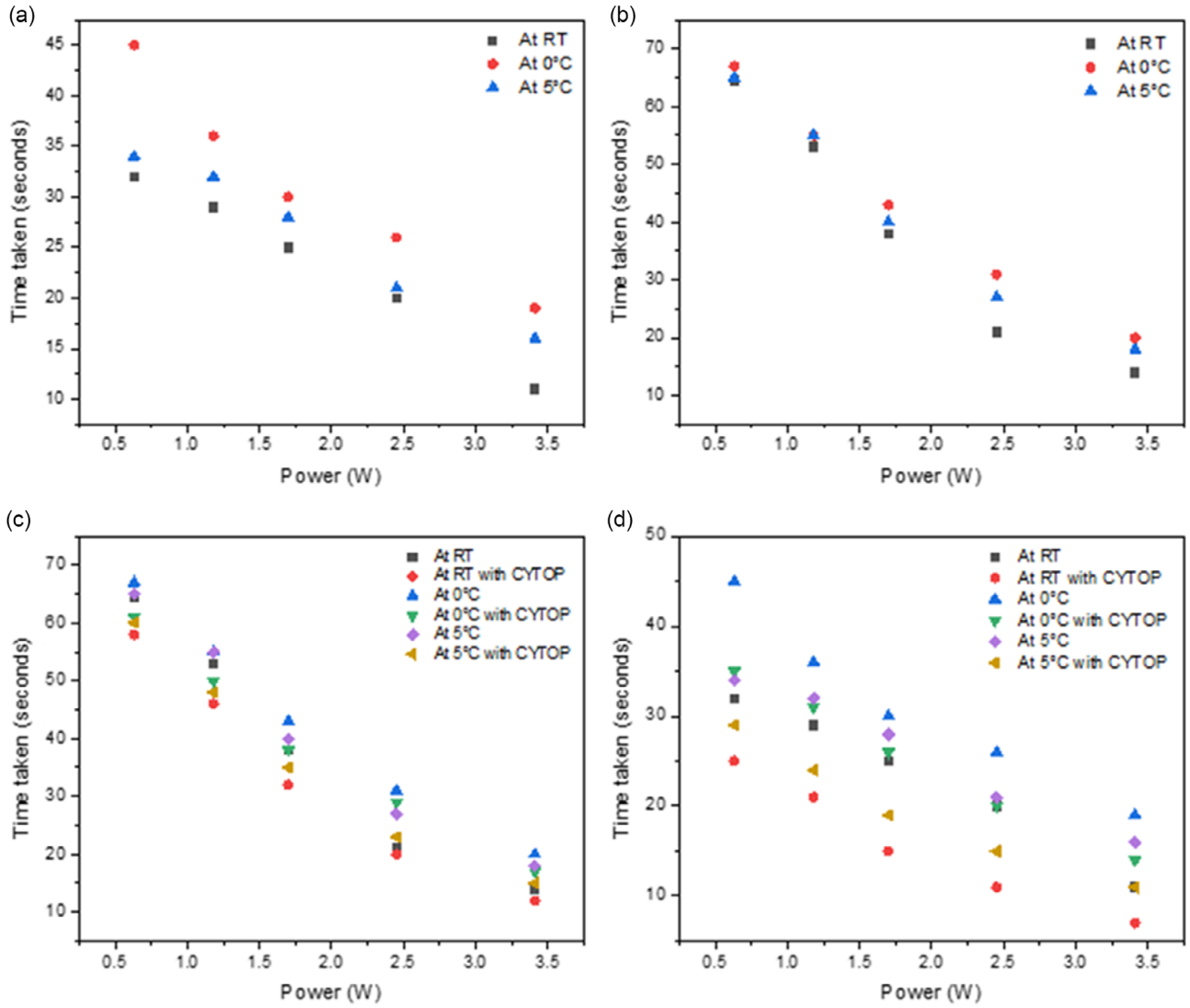

Figure 14. Illustrations of the de-fogging process for 28 MHz ZnO/glass SAW devices. a) 1 min exposure to humid air; b) 10 min exposure to humid air. De-fogging process for 9 MHz ZnO/glass SAW device: c) 1 min exposure to humid air. d) 10 min exposure to humid air. Reproduced (Adapted) with permission.[72] Copyright 2024, Elsevier.

agitation will propagate along the surface and drive away the fogging from the surface. Ong et al.[72] reported the use of both 9.88 and 27.92 MHz ZnO/glass SAW devices to realize de-fogging by pre-exposing the SAW devices to a humid air flow for 1 and 10 min. They evaluated the effects of surface treatment (using CYTOP®) and different temperature conditions (RT, 0 and 5 °C) on de-fogging performance. Results showed that the time taken to fulfil de-fogging is decreased with the increase of RF powers for both frequencies as shown in **Figure 14**. Also, it was noted that the time taken to remove fog upon 10 min exposure to humid air was much longer than that for 1 min, mainly due to the significantly higher amounts of condensates on the sample surface. In terms of temperature effects, it was found that a much longer time was required to remove at near 0 °C becasue more condensates were formed. It was noted that when RF power was applied onto the SAW device, the mechanical vibrations from the SAWs induce internal acoustic streaming in the fog, and a strong localized acoustothermal effect was also generated.[65,67] As the waves propagate on the surface of the ZnO/glass SAW device, they drive away the fog or evaporate them effectively, thus achieving the de-fogging effect. Authors also noted that CYTOP contributed to prompt the de-fogging process more effectively than the untreated ZnO/glass SAW devices.

6. Conclusions and Future Aspects

Concerns about fogging and icing issues in glass materials applications are significant and must be addressed. Various effective implementation methods have been thoroughly explored, including passive approaches like hydrophobic surface treatments and active strategies involving ultrasounds, chemical treatments, heat treatment, and mechanical means. However, these solutions are not deemed to be feasible in the long run as surface coatings may

lose their hydrophobicity after prolonged periods or instability upon exposure to extreme weather conditions. Unfortunately, the use of chemicals, particularly fluorine-containing polymers and molecules, brings up environmental issues in the long run. With these shortcomings, SAW technology, especially thin-film-based SAW devices, has been implemented to tackle these issues due to its easy operation, repeatability, reliability, high precision, and high throughput. Moreover, using microelectromechanical systems (MEMS) processes, it is easy to implement ultrahigh frequencies.

Various future advances can be explored using ZnO/glass SAW devices for functionalizing anti-fogging, de-fogging, anti-icing, and de-icing for ice mitigation. New methodologies, theoretical analysis and industry explorations, are still needed. Future lines of research and development are expected to proceed in the following directions. 1) Optimization of the electromechanical transduction efficiency and improving focusing effects to further enhance the acoustic streaming. It is necessary to characterize and study particle/surface systems in more realistic environments. Moreover, since the interaction between SAW and liquid is nonlinear, and the response involves time and length scales that differ by several orders of magnitude, it is worth finding ways and methods to analyze and simulate liquid/ice and solid substrate/ice behavior. At the same time, attention should also be paid to the influence of acoustothermal effects on the de-icing process and quantify to which extent propagating waves of different types affect the de-icing process. 2) More quantification testing in fogging and icing experiments on ZnO/glass SAW devices. Additional experimental results are needed, including ice adhesion test, droplet impacts, various hydrophobic surface treatments, wettability characterization of hydrophobic layers, and determination of parameters such as dynamic water contact angle parameters. These experiments will help to understand the behavior of the fog and the type of ice that forms on the glass surface, as well as how surface properties and environmental factors influence the effectiveness of ice mitigation using thin-film SAW on glass. Establishing standard conditions for reproducibility in icephobic experiments will enable benchmarking of SAW solutions. 3) Design, testing, and integration of WPT theory with SAW technology for actuation and sensing functions for various applications with ZnO/glass SAW devices. This will enable the dual functionality of the ZnO/glass SAW devices to realize and evaluate the rate of fog and ice formation via sensing and how this information can be used to adjust the amount of power required to remove fog or ice via actuation. Reducing energy costs for these functions through the enhancement of device efficiency should be also contemplated in the future. 4) Simulations and finite-element analysis to study the interaction mechanisms between SAW device and water droplet/ice particles to complement with obtained experimental results. This will allow the understanding of ice formation behavior upon SAW agitations (i.e., anti-icing conditions), as well as to better understand the mechanisms of energy transmission from substrate to already formed ice and link simulations to the observations obtained during experimentation. 5) Ensure radio frequency and electromagnetic compatibility, critical in various sector (such as aeronautical ones), which requires dedicated testing and validation to comply with the regulations for safety and reliability of aircraft systems. 6) Demonstration of compatibility with transparent protecting coatings. This aspect is urgent in real-scenario applications, given the low chemical and mechanical stability of ZnO due to erosion caused by ice. 7) Integration of passive and active methods as a way to promote hybridization with other systems, such as photothermal (this could be straightforward and interesting to reduce energy consumption) and low ice adhesion coatings. 8) Determine the optimum AW mode and characteristic for each environmental scenario and fogging/icing condition. Explore the possibility of adapting the wave mode and characteristics to the type and amount of ice. 9) Incorporate artificial intelligence, digital twins, and similar procedures to analyze and compute the huge variability caused by icing. This is particularly relevant for sensing and to complement current and future de-icing technologies, enabling their operation in a smart and automatic way. 10) Extend the technology to substrate materials other than glass (e.g., transparent polymers, composites). Attenuation and high acoustic impedance are constrains for the use of SAWs. Manufacturing laminates or special structures combining different materials can be an option to reduce costs and provide flexibility and other properties required for specific applications. 11) One key future development is the practical applications of monitoring and wireless systems, as well as the integration of de-icing and anti-icing technologies. These are crucial for the commercialization, depending on the areas of exploitation. For instance, wireless functions could be more important for transport and wind energy. However, there are a lot of challenges with applying the wireless functions, which need more extensive research. Multifunctional/transparency are also crucial for lens, smart screens, and solar panels. The durability and energy efficiency are needed for these applications.

Acknowledgements

This work was supported by the UK Fluids Network Special Interest Group of Acoustofluidics (EP/N032861/1), EPSRC Centre for Doctoral Training in Renewable Energy Northeast Universities (ReNU) for funding through grant EP/S023836/1, International Exchange Grant (IEC/NSFC/201078) through Royal Society and the Natural Science Foundation of China (NSFC), the EU H2020 program under grant agreement 899352 (FETOPEN-01-2018-2019-2020 – SOUNDofICE), PID2022-143120OB-I00, PCI2024-153451 (m-era.net 3, GA 958174), and TED2021-130916B-I00 funded by MCIN/AEI/10.13039/501100011033 and by "ERDF (FEDER)," A way of making Europe, Fondos NextgenerationEU, and Plan de Recuperación, Transformación y Resiliencia."

Conflict of Interest

The authors declare no conflict of interest.

Author Contributions

Hui Ling Ong: investigation (lead); methodology (lead); visualization (lead); writing—original draft (lead); **Zhangbin Ji**: visualization (equal); writing—review and editing (equal); **Luke Haworth**: visualization (equal); writing—review and editing (equal). **Yihao Guo**: visualization (equal). **Jaime del Moral**: visualization (lead); writing—review and editing (lead); **Stefan Jacob**: conceptualization (lead); supervision (lead); validation (lead); visualization (lead); writing—review and editing (lead). **Ana Borras**: conceptualization (lead); supervision (lead); validation (lead); visualization (lead); writing—review and editing (lead). **Agustin R. Gonzalez-Elipe**:

conceptualization (lead); validation (lead); visualization (lead); writing—review and editing (lead). **Jikai Zhang**: writing—review and editing (supporting). **Jian Zhou**: supervision (equal); validation (equal); writing—review and editing (equal). **Glen Mchale**: validation (lead); writing—review and editing (lead). **Yong-Qing Fu**: conceptualization (lead); resources (lead); supervision (lead); validation (lead); writing—review and editing (lead).

Keywords

frosting and icing, ice monitoring, ice protections, piezoelectric films, surface acoustic waves, ZnO

Received: September 11, 2024
Revised: November 17, 2024
Published online: January 28, 2025

[1] J. Zhou, X. L. He, W. B. Wang, Q. Zhu, W. P. Xuan, H. Jin, S. R. Dong, M. De Wang, J. K. Luo, *IEEE Electron Device Lett.* **2013**, *34*, 1319.
[2] J. Lim, C. Kang, K. Kim, I. Park, D. Hwang, S. Park, *Adv. Mater.* **2006**, *18*, 2720.
[3] J. C. Mauro, E. D. Zanotto, *Int. J. Appl. Glass Sci.* **2014**, *5*, 313.
[4] R. Rajaramakrishna, J. Kaewkhao, *KnE Soc. Sci.* **2019**, *3*, 796.
[5] J. Zhou, X. Z. Wu, D. B. Xiao, M. Zhuo, H. Jin, J. K. Luo, Y. Q. Fu, *Surf. Coat. Technol.* **2017**, *320*, 39.
[6] W.-B. Wang, H. Gu, X.-L. He, W.-P. Xuan, J.-K. Chen, X.-Z. Wang, J.-K. Luo, *Chin. Phys. B* **2015**, *24*, 057701.
[7] E. Axinte, *Mater. Des.* **2011**, *32*, 1717.
[8] K. Kasahara, T. Waku, P. W. Wilson, T. Tonooka, Y. Hagiwara, *Biomolecules* **2020**, *10*, 259.
[9] L. Tian, Z. Zhang, X. Jiang, L. Shu, J. Hu, H. Qin, presented at *ICHVE 2018 in Athens, Greece, September 10-13, 2018 IEEE Int. Conf. High Volt. Eng. Appl.*, February **2019**, https://doi.org/10.1109/ICHVE.2018.8642201.
[10] X. Du, Z. Yang, Z. Jin, Y. Zhu, Z. Zhou, Z. Zhou, *Proc. Inst. Mech. Eng., Part D* **2020**, *234*, 1480.
[11] A. Ene, C. Teodosiu, *IOP Conf. Ser.: Earth Environ. Sci.* **2021**, *664*, 012071.
[12] I. R. Durán, J. Profili, L. Stafford, G. Laroche, *Prog. Org. Coat.* **2020**, *141*, 105401.
[13] J. Carroll, *Natural Gas Hydrates*, Gulf Publishing Company, Houston, Texas **2020**, pp. 307–345, https://doi.org/10.1016/B978-0-12-821771-9.00010-0.
[14] Z. Zhang, S. Lv, S. Mehendale, L. Yan, H. Yuan, J. Tian, *Authorea* **2020**, *1*, 30.
[15] K. Xu, J. Hu, L. Shu, X. Jiang, Z. Huang, *AIP Adv.* **2018**, *8*, 35113.
[16] C. Liu, Z. Tian, Y. Zhao, X. Zeng, *IOP Conf. Ser.: Earth Environ. Sci.* **2020**, *514*, 032011.
[17] C. Liu, Y. Zhao, Z. Tian, H. Zhou, *Aerosol Air Qual. Res.* **2021**, *21*, 200361.
[18] S. Zang, M. Ding, D. Smith, P. Tyler, T. Rakotoarivelo, M. A. Kaafar, *IEEE Veh. Technol. Mag.* **2019**, *14*, 103.
[19] I. Gultepe, R. Tardiff, S. C. Michaelides, J. Cermak, A. Bott, J. Bendix, M. D. Muller, M. Pagowski, B. Hansen, G. Ellrod, W. Jacobs, G. Toth, S. G. Cober, *Pure Appl. Geophys.* **2007**, *164*, 1121.
[20] W. Li, C. Lin, W. Ma, Y. Li, F. Chu, B. Huang, S. Yao, *Cell Rep. Phys. Sci.* **2021**, *2*, 100435.
[21] G. P. Smestad, T. A. Germer, H. Alrashidi, E. F. Fernández, S. Dey, H. Brahma, N. Sarmah, A. Ghosh, N. Sellami, I. A. I. Hassan, M. Desouky, A. Kasry, B. Pesala, S. Sundaram, F. Almonacid, K. S. Reddy, T. K. Mallick, L. Micheli, *Sci. Rep.* **2020**, *10*, 58.
[22] B. R. Paudyal, S. R. Shakya, D. P. Paudyal, D. Das Mulmi, *Renewables Wind Water Sol.* **2017**, *4*, pp. 1–8.
[23] M. R. Maghami, H. Hizam, C. Gomes, M. A. Radzi, M. I. Rezadad, S. Hajighorbani, *Renewable Sustainable Energy Rev.* **2016**, *59*, 1307.
[24] A. Hussain, A. Batra, R. Pachauri, *Renewables Wind Water Sol.* **2017**, *4*.
[25] B. P. Jelle, T. Gao, S. A. Mofid, T. Kolås, P. M. Stenstad, S. Ng, *Proc. Eng.* **2016**, *145*, 699.
[26] Y.-H. Jia, F.-F. Li, K. Fang, G.-Q. Wang, J. Qiu, *J. Appl. Meteorol. Climatol.* **2021**, *60*, 1373.
[27] M. Zhang, F. He, C. Li, J. Li, Z. Zeng, K. Yu, P. Yuan, *J. Phys. D: Appl. Phys.* **2021**, *54*, 395301.
[28] H. Czyż, T. Markowski, H. Czy, *Aviation* **2007**, *XI*, 26.
[29] I. Haechler, N. Ferru, G. Schnoering, E. Mitridis, T. M. Schutzius, D. Poulikakos, *Nat. Nanotechnol.* **2023**, *18*, 137.
[30] J. Shi, S. Ke, F. Wang, W. Wang, C. Wang, *Chem. Eng. J.* **2024**, *481*, 148265.
[31] F. T. Baheri, L. D. Poulikakos, D. Poulikakos, T. M. Schutzius, *Constr. Build. Mater.* **2021**, *298*, 123851.
[32] N. Dalili, A. Edrisy, R. Carriveau, *Renewable Sustainable Energy Rev.* **2009**, *13*, 428.
[33] G. Heydari, E. Thormann, M. Järn, E. Tyrode, P. M. Claesson, *J. Phys. Chem. C* **2013**, *117*, 21752.
[34] Y. Li, D. R. Dekel, O. Manor, *ACS Appl. Mater. Interfaces* **2021**, *13*, 59471.
[35] S. Milles, M. Soldera, B. Voisiat, A. F. Lasagni, *Sci. Rep.* **2019**, *9*, 1.
[36] Y. Zhuo, V. Håkonsen, Z. He, S. Xiao, J. He, Z. Zhang, *ACS Appl. Mater. Interfaces* **2018**, *10*, 11972.
[37] K. K. Varanasi, T. Deng, J. D. Smith, M. Hsu, N. Bhate, *Appl. Phys. Lett.* **2010**, *97*, 234102.
[38] X. Tan, Y. Zhang, X. Liu, S. Xi, Z. Yan, Z. Liu, T. Shi, G. Liao, *Surf. Coat. Technol.* **2021**, *405*, 126568.
[39] J. Li, E. Ueda, D. Paulssen, P. A. Levkin, *Adv. Funct. Mater.* **2019**, *29*, 1802317.
[40] H. Niemelä-Anttonen, H. Koivuluoto, M. Tuominen, H. Teisala, P. Juuti, J. Haapanen, J. Harra, C. Stenroos, J. Lahti, J. Kuusipalo, J. M. Mäkelä, P. Vuoristo, *Adv. Mater. Interfaces* **2018**, *5*, 1800828.
[41] H. He, Z. Guo, *iScience* **2021**, *24*, 103357.
[42] A. J. Meuler, J. D. Smith, K. K. Varanasi, J. M. Mabry, G. H. McKinley, R. E. Cohen, *ACS Appl. Mater. Interfaces* **2010**, *2*, 3100.
[43] Y. Liu, L. J. Bond, H. Hu, *AIAA J.* **2017**, *55*, 1602.
[44] M. Yamazaki, A. Jemcov, H. Sakaue, *Aerospace* **2021**, *8*, 188.
[45] H. Dai, C. Zhu, H. Zhao, S. Liu, *Appl. Sci.* **2021**, *11*, 5693.
[46] P.-O. A. Borrebæk, S. Rønneberg, B. P. Jelle, A. Klein-Paste, Z. Zhang, J. He, *J. Adhes. Sci. Technol.* **2021**, *35*, 1087.
[47] P.-O. A. Borrebæk, B. P. Jelle, Z. Zhang, *Sol. Energy Mater. Sol. Cells* **2020**, *206*, 110306.
[48] Y. Huang, P. K. Das, V. R. Bhethanabotla, *Sens. Actuators Rep.* **2021**, *3*, 100041.
[49] D. B. Go, M. Z. Atashbar, Z. Ramshani, H.-C. Chang, *Anal. Methods* **2017**, *9*, 4112.
[50] D. Mandal, S. Banerjee, *Sensors* **2022**, *22*, 820.
[51] Y. Yang, C. Dejous, H. Hallil, *Micromachines* **2023**, *14*, 43.
[52] S. Damiati, U. B. Kompella, S. A. Damiati, R. Kodzius, *Genes* **2018**, *9*, 103.
[53] H. Fallahi, J. Zhang, H.-P. Phan, N.-T. Nguyen, *Micromachines* **2019**, *10*, 830.
[54] P. Delsing, A. N. Cleland, M. J. A. Schuetz, J. Knörzer, G. Giedke, J. I. Cirac, K. Srinivasan, M. Wu, K. C. Balram, C. Bäuerle, T. Meunier, C. J. B. Ford, P. V. Santos, E. Cerda-Méndez, H. Wang, H. J. Krenner, E. D. S. Nysten, M. Weiß, G. R. Nash, L. Thevenard, C. Gourdon, P. Rovillain, M. Marangolo, J.-Y. Duquesne, G. Fischerauer, W. Ruile, A. Reiner, B. Paschke, D. Denysenko, D. Volkmer, A. Wixforth, et al., *J. Phys. D: Appl. Phys.* **2019**, *52*, 353001.

[55] Y. Q. Fu, J. K. Luo, N. T. Nguyen, A. J. Walton, A. J. Flewitt, X. T. Zu, Y. Li, G. Mchale, A. Matthews, E. Iborra, H. Du, W. I. Milne, *Prog. Mater. Sci.* **2017**, *89*, 31.
[56] B. Liu, X. Chen, H. Cai, M. Mohammad Ali, X. Tian, L. Tao, Y. Yang, T. Ren, *J. Semicond.* **2016**, *37*, 021001.
[57] V. Naresh, N. Lee, *Sensors* **2021**, *21*, 1109.
[58] X. L. He, J. Zhou, W. B. Wang, W. P. Xuan, X. Yang, H. Jin, J. K. Luo, *J. Micromech. Microeng.* **2014**, *24*, 055014.
[59] L. Y. Yeo, J. R. Friend, *Annu. Rev. Fluid Mech.* **2014**, *46*, 379.
[60] G. L. Cote, R. M. Lec, M. V. Pishko, *IEEE Sens. J.* **2003**, *3*, 251.
[61] J. Friend, L. Y. Yeo, *Rev. Mod. Phys.* **2011**, *83*, 647.
[62] L. Y. Yeo, J. R. Friend, *Biomicrofluidics* **2009**, *3*, 012002.
[63] J. Li, M. H. Biroun, R. Tao, Y. Wang, H. Torun, N. Xu, M. Rahmati, Y. Li, D. Gibson, C. Fu, J. Luo, L. Dong, J. Xie, Y. Fu, *J. Phys. D: Appl. Phys.* **2020**, *53*, 355402.
[64] M. Safaei, H. A. Sodano, S. R. Anton, *Smart Mater. Struct.* **2019**, *28*, 113001.
[65] D. Yang, R. Tao, X. Hou, H. Torun, G. Mchale, J. Martin, Y. Fu, *Adv. Mater. Interfaces* **2021**, *8*, 2001776.
[66] L. Haworth, D. Yang, P. Agrawal, H. Torun, X. Hou, G. Mchale, Y. Fu, *Nanotechnol. Precis. Eng.* **2023**, *6*, 013007.
[67] D. Yang, L. Haworth, P. Agrawal, R. Tao, G. Mchale, H. Torun, J. Martin, J. Luo, X. Hou, Y. Fu, *Langmuir* **2022**, *38*, 11314.
[68] V. Daniliuk, Y. Xu, R. Liu, T. He, X. Wang, *Renewable Energy* **2020**, *145*, 2005.
[69] J. Del Moral, L. Montes, V. J. Rico-Gavira, C. López-Santos, S. Jacob, M. Oliva-Ramirez, J. Gil-Rostra, A. Fakhfouri, S. Pandey, M. Gonzalez Del Val, J. Mora, P. García-Gallego, P. F. Ibáñez-Ibáñez, M. A. Rodríguez-Valverde, A. Winkler, A. Borrás, A. R. González-Elipe, *Adv. Funct. Mater.* **2023**, *33*, 2209421.
[70] A. Karimzadeh, U. Weissker, J. Del Moral, A. Winkler, A. Borrás, A. R. González-Elipe, S. Jacob, *Adv. Mater. Technol.* **2024**, *9*, 2301749.
[71] S. Jacob, S. Pandey, J. D. Moral, A. Karimzadeh, J. Gil-Rostra, A. R. González-Elipe, A. Borrás, A. Winkler, *Adv. Mater. Technol.* **2023**, *8*, 2300263.
[72] H. L. Ong, D. Yang, H. Chen, J. Zhou, L. Haworth, J. Zhang, D. Gibson, P. Agrawal, H. Torun, Q. Wu, X. Hou, Y. Fu, *Mater. Chem. Phys.* **2023**, *304*, 127842.
[73] J. Zhou, Y. Guo, Y. Wang, Z. Ji, Z. Zhang, F. Zhou, J. Luo, R. Tao, J. Xie, J. Reboud G. McHale, S. Dong, J. Luo, H. Duan, Y. Q. Fu, *Appl. Phys. Rev.* **2023**, *10*, 021311.
[74] Y. Q. Fu, J. K. Luo, X. Y. Du, A. J. Flewitt, Y. Li, G. H. Markx, A. J. Walton, W. I. Milne, *Sens. Actuators, B* **2010**, *143*, 606.
[75] M. I. Jamil, A. Ali, F. Haq, Q. Zhang, X. Zhan, F. Chen, *Langmuir* **2018**, *34*, 15425.
[76] S. Yang, C. Wu, G. Zhao, J. Sun, X. Yao, X. Ma, Z. Wang, *Cell Rep. Phys. Sci.* **2021**, *2*, 100474.
[77] A. Dhyani, W. Choi, K. Golovin, A. Tuteja, *Matter* **2022**, *5*, 1423.
[78] S. Jung, M. Dorrestijn, D. Raps, A. Das, C. M. Megaridis, D. Poulikakos, *Langmuir* **2011**, *27*, 3059.
[79] L. Cao, A. K. Jones, V. K. Sikka, J. Wu, D. Gao, *Langmuir* **2009**, *25*, 12444.
[80] S. Farhadi, M. Farzaneh, S. A. Kulinich, *Appl. Surf. Sci.* **2011**, *257*, 6264.
[81] T.-S. Wong, S. H. Kang, S. K. Y. Tang, E. J. Smythe, B. D. Hatton, A. Grinthal, J. Aizenberg, *Nature* **2011**, *477*, 443.
[82] P. Kim, T. S. Wong, J. Alvarenga, M. J. Kreder, W. E. Adorno-Martinez, J. Aizenberg, *ACS Nano* **2012**, *6*, 6569.
[83] S. Ozbay, C. Yuceel, H. Y. Erbil, *ACS Appl. Mater. Interfaces* **2015**, *7*, 22067.
[84] M. J. Kreder, J. Alvarenga, P. Kim, J. Aizenberg, *Nat. Rev. Mater.* **2016**, *1*, 15003.
[85] H. Sojoudi, G. H. Mckinley, K. K. Gleason, *Mater. Horiz.* **2015**, *2*, 91.
[86] S. Yang, Q. Xia, L. Zhu, J. Xue, Q. Wang, Q. Chen, *Appl. Surf. Sci.* **2011**, *257*, 4956.
[87] J. Peng, B. Liu, S. H. Gao, K. Y. Zhu, Y. H. Zhao, X. H. Li, X. Y. Yuan, *Sci. China Technol. Sci.* **2020**, *63*, 960.
[88] B. Liu, K. Zhang, C. Tao, Y. Zhao, X. Li, K. Zhu, X. Yuan, *RSC Adv.* **2016**, *6*, 70251.
[89] S. Zhang, J. Huang, Y. Cheng, H. Yang, Z. Chen, Y. Lai, *Small* **2017**, *13*, 1701867.
[90] E. Corsini, R. W. Luebke, D. R. Germolec, J. C. Dewitt, *Toxicol. Lett.* **2014**, *230*, 263.
[91] X. Zhao, B. Khatir, K. Mirshahidi, K. Yu, J. N. Kizhakkedathu, K. Golovin, *ACS Nano* **2021**, *15*, 13559.
[92] J. Sarma, L. Zhang, Z. Guo, X. Dai, *Chem. Eng. J.* **2022**, *431*, 133475.
[93] X. Hao, Z. Sun, S. Wu, T. Wang, Y. Liu, Y. Wu, X. He, Q. Liu, F. Zhou, *Adv. Mater. Interfaces* **2022**, *9*, 2200160.
[94] S. Li, Y. Hou, M. Kappl, W. Steffen, J. Liu, H. Butt, *Adv. Mater.* **2022**, *34*, 2203242.
[95] K. Golovin, S. P. R. Kobaku, D. H. Lee, E. T. DiLoreto, J. M. Mabry, A. Tuteja, *Sci. Adv.* **2016**, *2*, https://doi.org/10.1126/SCIADV.1501496/SUPPL_FILE/1501496_SM.PDF.
[96] G. Fortin, J.-L. Laforte, A. Ilinca, *Int. J. Therm. Sci.* **2006**, *45*, 595.
[97] Y. Yin, L. Cheng, W. Wang, Y. Zhang, Y. Liang, *AIP Adv.* **2021**, *11*, 115028.
[98] I. V. Roisman, C. Tropea, *Curr. Opin. Colloid Interface Sci.* **2021**, *53*, 101400.
[99] Y. Liu, W. L. Chen, L. J. Bond, H. Hu, *AIP Conf. Proc.* **2014**, *1581*, 1757.
[100] Y. Wu, Z. Ma, S. Lu, L. Qin T. Zheng, G. Dong, *Langmuir* **2024**, *40*, 19853.
[101] K. Zhang, S. Huang, Q. Zhang, H. Zhu, S. Zhu, *Can. J. Chem. Eng.* **2023**, *101*, 4979.
[102] J. Bian, T. Yang, C. Yuan, H. Ge, Y. Chen, *Appl. Phys. A* **2014**, *116*, 79.
[103] H. Kwon, C. Y. Gao, X. Tang, J. Hong, C. E. Park, H. Kong, S. H. Kim, H. Yang, *Org. Electron.* **2020**, *77*, 105485.
[104] Y. Li, C. Liu, Y. Xu, T. Minari, P. Darmawan, K. Tsukagoshi, *Org. Electron.* **2012**, *13*, 815.
[105] P. Dimitrakellis, E. Gogolides, *Adv. Colloid Interface Sci.* **2018**, *254*, 1.
[106] A. Terriza, R. Álvarez, A. Borrás, J. Cotrino, F. Yubero, A. R. González-Elipe, *J. Colloid Interface Sci.* **2012**, *376*, 274.
[107] A. Terriza, M. Macías-Montero, M. C. López-Santos, F. Yubero, J. Cotrino, A. R. González-Elipe, *Plasma Process. Polym.* **2014**, *11*, 289.
[108] D. Kontziampasis, G. Boulousis, A. Smyrnakis, K. Ellinas, A. Tserepi, E. Gogolides, *Microelectron. Eng.* **2014**, *121*, 33.
[109] V. J. Rico, C. L. Santos, M. Villagra, J. P. Espinos, L. A. Angurel, A. Borras, A. R. Gonzalez-Elipe, *Langmuir* **2019**, *35*, 6483.
[110] M. Psarski, G. Celichowski, E. Bystrzycka, D. Pawlak, J. Grobelny, M. Cichomski, *Mater. Chem. Phys.* **2018**, *204*, 305.
[111] L. W. Teunissen, M. M. J. Smulders, H. Zuilhof, *Langmuir* **2023**, *39*, 7613.
[112] J. Zhou, L. Tang, *Prog. Org. Coat.* **2024**, *189*, 108342.
[113] A. Lafuma, D. Quéré, *Europhys. Lett.* **2011**, *96*, 56001.
[114] M. J. Kreder, J. Alvarenga, P. Kim, J. Aizenberg, *Nat. Rev. Mater.* **2016**, *1*, 15003.
[115] N. R. Geraldi, J. H. Guan, L. E. Dodd, P. Maiello, B. B. Xu, D. Wood, M. I. Newton, G. G. Wells, G. Mchale, *Sci. Rep.* **2019**, *9*, 13280.
[116] M. Villegas, Y. Zhang, N. Abu Jarad, L. Soleymani, T. F. Didar, *ACS Nano* **2019**, *13*, 8517.
[117] S. S. Latthe, R. S. Sutar, A. K. Bhosale, S. Nagappan, C.-S. Ha, K. K. Sadasivuni, S. Liu, R. Xing, *Prog. Org. Coat.* **2019**, *137*, 105373.
[118] L. Wang, T. J. Mccarthy, *Angew. Chem., Int. Ed.* **2016**, *55*, 244.
[119] B. J. Melde, A. P. Malanoski, M. H. Moore, B. J. Johnson, *Polym. Int.* **2021**, *70*, 701.

[120] P. Lv, Y. Zhang, D. Han, H. Sun, *Adv. Mater. Interfaces* **2021**, *8*, 2100043.
[121] D. Tripathi, P. Ray, A. V. Singh, V. Kishore, S. L. Singh, *Coatings* **2023**, *13*, 1095.
[122] W. Cui, T. A. Pakkanen, *J. Colloid Interface Sci.* **2020**, *558*, 251.
[123] K. E. Dehm, T. Walter, M. Weichselgartner, R. W. Crisp, K. Wommer, M. Aust, N. Vogel, *Adv. Mater. Interfaces* **2023**, *10*, 2202032.
[124] V. Rico, J. Mora, P. García, A. Agüero, A. Borrás, A. R. González-Elipe, C. López-Santos, *Appl. Mater. Today* **2020**, *21*, 100815.
[125] I. J. Gresham, C. Neto, *Adv. Colloid Interface Sci.* **2023**, *315*, 102906.
[126] L. Chen, S. Huang, R. H. A. Ras, X. Tian, *Nat. Rev. Chem.* **2023**, *7*, 123.
[127] L. Zhang, Z. Guo, J. Sarma, X. Dai, *ACS Appl. Mater. Interfaces* **2020**, *12*, 20084.
[128] A. K. Halvey, B. Macdonald, K. Golovin, M. Boban, A. Dhyani, D. H. lee, J. W. Gose, S. L. Ceccio A. Tuteja, *ACS Appl. Mater. Interfaces* **2021**, *13*, 53171.
[129] H. Cha, H. Vahabi, A. Wu, S. Chavan, M. K. Kim, S. Sett, S. A. Bosch, W. Wang, A. K. Kota, N. Miljkovic, *Sci. Adv.* **2020**, *6*, https://doi.org/10.1126/SCIADV.AAX0746/SUPPL_FILE/AAX0746_SM.PDF.
[130] H. Vahabi, S. Vallabhuneni, M. Hedayati, W. Wang, D. Krapf, M. J. Kipper, N. Miljkovic, A. K. Kota, *Matter* **2022**, *5*, 4502.
[131] D. Yang, L. Haworth, P. Agrawal, R. Tao, G. Mchale, H. Torun, J. Martin, J. Luo, X. Hou, Y. Fu, *Langmuir* **2022**, *38*, 11314.
[132] Z. Han, X. Feng, Z. Jiao, Z. Wang, J. Zhang, J. Zhao, S. Niu, L. Ren, *RSC Adv.* **2018**, *8*, 26497.
[133] W. Shi, L. Wang, Z. Guo, Y. Zheng, *Adv. Mater. Interfaces* **2015**, *2*, 1500352.
[134] H. Gao, Y. Jian, Y. Yan, *Soft Matter* **2021**, *17*, 447.
[135] R. Pradhan, H. S. Grewal, *Small Methods* **2024**, *8*, 2400459.
[136] M. Domke, G. Sonderegger, E. Kostal, V. Matylitsky, S. Stroj, *Appl. Phys. A* **2019**, *125*, 675.
[137] J. Imgrunt, K. Chakanga, K. von Maydell, U. Teubner, *Appl. Phys. A* **2017**, *123*, 776.
[138] A. Ouchene, G. Mollon, M. Ollivier, X. Sedao, A. Pascale-Hamri, G. Dumazer, E. Serris, *Appl. Surf. Sci.* **2023**, *630*, 157490.
[139] Y. Yalikun, Y. Hosokawa, T. Iino, Y. Tanaka, *Lab Chip* **2016**, *16*, 2427.
[140] H. M. Lee, J. H. Choi, S. J. Moon, *Int. J. Precis. Eng. Manuf. Green Technol.* **2021**, *8*, 375.
[141] X. D. Cao, B. H. Kim, C. N. Chu, *Precis. Eng.* **2009**, *33*, 459.
[142] J. Arrés Chillón, B. Paulillo, P. Mazumder, V. Pruneri, *ACS Appl. Nano Mater.* **2022**, *5*, 17606.
[143] E. Yu, S.-C. Kim, H. J. Lee, K. H. Oh, M.-W. Moon, *Sci. Rep.* **2015**, *5*, 9362.
[144] F. Wang, Y. Zhuo, Z. He, S. Xiao, J. He, Z. Zhang, *Adv. Sci.* **2021**, *8*, 2101163.
[145] M. M. Ahmad, A. Eshaghi, *Prog. Org. Coat* **2018**, *122*, 199.
[146] K.-K. Kwon, K. Y. Song, J. M. Seo, C. N. Chu, S.-H. Ahn, *J. Mater. Process. Technol.* **2021**, *291*, 117046.
[147] S.-H. Lee, J. Kim, M. Seong, S. Kim, H. Jang, H. W. Park, H. E. Jeong, *Compos. Sci. Technol.* **2022**, *217*, 109086.
[148] H. He, W. Huang, Z. Guo, *Mater. Today Phys.* **2023**, *30*, 100927.
[149] M. Kim, J. Lee, J. Nam, *Adv. Sci.* **2019**, *6*, 1900471.
[150] G. Baffou, I. Bordacchini, A. Baldi, R. Quidant, *Light: Sci. Appl.* **2020**, *9*, 108.
[151] W. Guo, C. Liu, N. Li, M. Xi, Y. Che, C. Jiang, S. Zhang, Z. Wang, *Nanoscale Adv.* **2022**, *4*, 2884.
[152] L. Zhang, B. Luo, K. Fu, C. Gao, X. Han, M. Zhou, T. Zhang, L. Zhong, Y. Hou, Y. Zheng, *Adv. Sci.* **2023**, *10*, 2304187.
[153] X. Guo, Q. Yang, H. Zheng, W. Dong, *Appl. Therm. Eng.* **2024**, *236*, 121723.
[154] K. Khaled, U. Berardi, *Energy Build.* **2021**, *244*, 111022.
[155] S.-L. Jia, H.-Z. Geng, L. Wang, Y. Tian, C.-X. Xu, P.-P. Shi, Z.-Z. Gu, X.-S. Yuan, L.-C. Jing, Z.-Y. Guo, J. Kong, *R. Soc. Open Sci.* **2018**, *5*, 172072.
[156] L. Cui, K. Cui, H. Ci, K. Zheng, H. Xie, X. Gao, Y. Zhang, Z. Liu, *Nanomaterials* **2019**, *9*, 558.
[157] Z. Li, Z. Zhen, M. Chai, X. Zhao, Y. Zhong, H. Zhu, *Small* **2020**, *16*, 1905945.
[158] Y. Wang, Y. Xue, Y. Sun, X. Sui, Y. Wang, W. Liang, Y. Wang, D. Zhu, H. Zhao, *Surf. Interfaces* **2023**, *42*, 103430.
[159] Y. Wang, K. Zhang, X. Cui, Z. Zhao, Z. Wang, G. Liu, Y. Zhang, Y. Zhu, J. Chen, S. Sun, X. Liu, H. Chen, *ACS Appl. Mater. Interfaces* **2024**, *16*, 41400.
[160] D. De Pauw, A. Dolatabadi, *J. Aircr.* **2016**, *54*, 490.
[161] H. Sun, G. Lin, H. Jin, X. Bu, C. Cai, Q. Jia, K. Ma, D. Wen, *Renewable Energy* **2021**, *179*, 1179.
[162] H. Habibi, L. Cheng, H. Zheng, V. Kappatos, C. Selcuk, T.-H. Gan, *Renewable Energy* **2015**, *83*, 859.
[163] E. A. Ash, A. A. Oliner, *Acoust. Surf. Waves* **1978**, *18*.
[164] R. P. Hodgson, M. Tan, L. Yeo, J. Friend, *Appl. Phys. Lett.* **2009**, *94*, 24102.
[165] Z. H. Shi, J. F. Zhang, Presented at *Proc. 2019 13th Symp. Piezoelectrcity, Acoust. Waves, Device Appl. SPAWDA 2019 in Harbin*, China, 11-14, January 2019, April **2019**, https://doi.org/10.1109/SPAWDA.2019.8681788.
[166] L. Shen, D. Li, Y. Shang, J. Wang, *Int. J. Refrig.* **2023**, *149*, 168.
[167] H. Ong, H. Pang, J. Zhou, R. Tao, P. Agrawal, H. Torun, K. Thummavichai, J. Luo, K. Tao, Q. Wu, H. Chang, Y.-Q. Fu, *Mater. Chem. Phys.* **2022**, *287*, 126290.
[168] X. Zeng, H. Ong, L. Haworth Y. Lu, D. Yang, M. Rahmati, Q. Wu, H. Torun, J. Martin, X. Hou, X. Lv, W. Yuan, Y. He, Y. Q. Fu, *ACS Appl. Mater. Interfaces* **2023**, *15*, 35648.
[169] G. H. Haertling, *J. Am. Ceram. Soc.* **1999**, *82*, 797.
[170] S. A. Hasan, *Ph.D. Thesis*, Northumbria University, Newcastle, UK **2019**.
[171] K. K. Sappati, S. Bhadra, *Sensors* **2018**, *18*, 3605.
[172] K. S. Ramadan, D. Sameoto, S. Evoy, *Smart Mater. Struct.* **2014**, *23*, 033001.
[173] H. Wei, H. Wang, Y. Xia, D. Cui, Y. Shi, M. Dong, C. Liu, T. Ding, J. Zhang, Y. Ma, N. Wang, Z. Wang, Y. Sun, R. Wei, Z. Guo, *J. Mater. Chem. C* **2018**, *6*, 12446.
[174] C. Caliendo, F. Laidoudi, *Sensors* **2020**, *20*, 1380.
[175] K. Tian, B. Tudu, A. Tiwari, *Vacuum* **2017**, *146*, 483.
[176] G. A. Kumar, M. V. R. Reddy, K. N. Reddy, *IOP Conf. Ser. Mater. Sci. Eng.* **2015**, *73*, 012133.
[177] X. García-Casas, F. J. Aparicio, J. Budagosky, A. Ghaffarinejad, N. Orozco-Corrales, K. Ostrikov, J. R. Sánchez-Valencia, Á. Barranco, A. Borrás, *Nano Energy* **2023**, *114*, 108686.
[178] H.-F. Pang, L. Garcia-Gancedo, Y. Q. Fu, S. Porro, Y.-W. Gu, J. K. Luo, X.-T. Zu, F. Placido, J. I. B. Wilson, A. J. Flewitt, W. I. Milne, *Phys. Status Solidi* **2013**, *210*, 1575.
[179] P. Romero-Gómez, J. Toudert, J. R. Sánchez-Valencia, A. Borrás, A. Barranco, A. R. Gonzalez-Elipe, *J. Phys. Chem. C* **2010**, *114*, 20932.
[180] C. Belkhaoui, N. Mzabi, H. Smaoui, *Mater. Res. Bull.* **2019**, *111*, 70.
[181] Q. Fan, D. Li, J. Li, C. Wang, *J. Alloys Compd.* **2020**, *829*, 154483.
[182] Y. C. Yang, C. Song, X. H. Wang, F. Zeng, F. Pan, *Appl. Phys. Lett.* **2008**, *92*, 012907.
[183] W. Xuan, M. He, N. Meng, X. He, W. Wang, J. Chen, T. Shi, T. Hasan, Z. Xu, Y. Xu, J. K. Luo, *Sci. Rep.* **2014**, *4*, 7206.
[184] W. Wang, X. He, J. Zhou, H. Gu, W. Xuan, J. Chen, X. Wang, J. Luo, *J. Electrochem. Soc.* **2014**, *161*, B230.
[185] X. L. He, J. Zhou, W. B. Wang, W. P. Xuan, D. J. Li, S. R. Dong, H. Jin, Y. Xu, J. K. Luo, *Behav. Brain Sci.* **2014**, *1659*, 75.

[186] K.-H. Bang, D.-K. Hwang, M.-C. Jeong, K.-S. Sohn, J.-M. Myoung, *Solid State Commun.* **2003**, *126*, 623.
[187] Y. N. Chanchangi, A. Ghosh, S. Sundaram, T. K. Mallick, *Renewable Sustainable Energy Rev.* **2020**, *121*,109704.
[188] M. P. Nair, A. J. T. Teo, K. H. H. Li, *Micromachines* **2022**, *13*, 24.
[189] S. M. Garner, X. Li, M. H. Huang, *Flexible Glass* **2017**, *1*,1.
[190] J. Wu, C. Yin, J. Zhou, H. Li, Y. Liu, Y. Shen, S. Garner, Y. Fu, H. Duan, *ACS Appl. Mater. Interfaces* **2020**, *12*, 39817.
[191] C. Yin, J. Wu, J. Zhou, D. Zhang, Z. Liu, X. Liu, L. Liu, Z. Zhan, S. Garner, Y. Fu, *Sens. Actuators, A* **2021**, *321*, 112590.
[192] J. Chen, H. Guo, X. He, W. Wang, W. Xuan, H. Jin, S. Dong, X. Wang, Y. Xu, S. Lin, S. Garner, J. Luo, *J. Micromech. Microeng.* **2015**, *25*, 115005.
[193] J. Chen, X. He, W. Wang, W. Xuan, J. Zhou, X. Wang, S. R. Dong, S. Garner, P. Cimo, J. K. Luo, *J. Mater. Chem. C* **2014**, *2*, 9109.
[194] Z. Ji, J. Zhou, H. Lin, J. Wu, D. Zhang, S. Garner, A. Gu, S. Dong, Y. Fu, H. Duan, *Microsyst. Nanoeng.* **2021**, *7*, 97.
[195] Z. Ji, J. Zhou, Y. Guo, Y. Xia, A. Abkar, D. Liang, Y. Fu, *Microsyst. Nanoeng.* **2024**, *10*, 94.
[196] H. Li, K. Mou, B. Peng, Y. Deng, X. Liu, S. Ta, Z. Yang, T. Sun, F. Zhang, Q. Li, G. Xiao, T. Fu, Y. Chen, H. Karimi-Maleh, *J. Nanomater.* **2022**, *2022*, 2599390.
[197] J. Zhou, J. Zheng, X. Shi, Z. Che, J. Wu, S. Xiong, J. Luo, S. Dong, H. Jin, H. Duan, Y. Q. DuanFu, *J. Electrochem. Soc.* **2019**, *166*, B432.
[198] P. Wang, W. Zhou, Y. Bao, H. Li, *Struct. Control Health Monit.* **2018**, *25*, e2138.
[199] P. Schulmeyer, M. Weihnacht, H. Schmidt, *Sensors* **2024**, *24*, 2292.
[200] V. Anisimkin, V. Kolesov, A. Kuznetsova, E. Shamsutdinova, I. Kuznetsova, *Sensors* **2021**, *21*, 919.
[201] V. I. Anisimkin, N. V. Voronova, *Ultrasonics* **2021**, *116*, 106496.
[202] S. Pandey, J. del Moral, S. Jacob, L. Montes, J. GilHRostra, A. Frechilla, A. Karimzadeh, V. J. Rico, R. Kantar, N. Kandelin, C. L. Santos, H. Koivuluoto, L. Angurel, A. Winkler, A. Borras, A. R. G. Elipe, Mechanisms of De-icing by Surface Rayleigh and Plate Lamb Acoustic Waves **2024**, https://arxiv.org/abs/2408.05465v1 (accessed: September 2024).
[203] Y. Wang, Q. Zhang, R. Tao, J. Xie, P. Canyelles-Pericas, H. Torun, J. Reboud, G. Mchale, L. E. Dodd, X. Yang, J. Luo, Q. Wu, Y. Fu, *ACS Appl. Mater. Interfaces* **2021**, *13*, 16978.
[204] X. Zeng, Z. Yan, Y. Lu, Y. Q. Fu, X. Lv, W. Yuan, Y. He, *Langmuir* **2021**, *37*, 11851.
[205] K. N. Nampoothiri, A. Nath, N. S. Satpathi, A. K. Sen, *Langmuir* **2023**, *39*, 3934.
[206] H. Ong, F. Yang, L. Haworth, C. Zhang, J. Zhang, H. Wu, J. Luo, Q. Wu, Y. Q. Fu, *ACS Appl. Mater. Interfaces* **2024**, *16*, 62999.
[207] D. Trevett, P. Trevett, *Ultrasonically clearing precipitation, WO2015011064A1*, January **2015**.
[208] M. Baudoin, R. Chutani, F. Bretagnol, A. Peret, *Device for cleaning an optical surface US20240042969A1*, February **2024**.

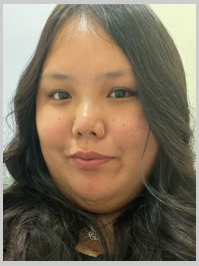

Hui Ling Ong obtained her Ph.D. in electrical engineering from the University of Northumbria at Newcastle, UK, in 2024. Currently, she is a postdoctoral researcher in mechanical engineering at the University of Northumbria at Newcastle, UK. Her main research focuses on thin-film transparent SAW devices such as glass substrates to functionalize various applications such as active surface cleaning, anti- and de-icing functions, and UV sensing. Her research also involved using thin-film SAW devices on silicon substrates to study bacterial growth and inactivation.

Zhangbin Ji received his B.S. from North University of China, China, in 2020. He is currently pursuing Ph.D. in the College of Mechanical and Vehicle Engineering, Hunan University, China. His research interests focus on flexible surface acoustic wave devices, sensors, and machine learning.

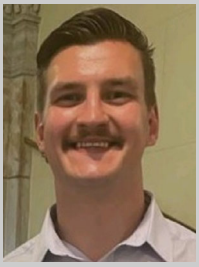

Luke Haworth has been a postdoctoral researcher at ESPCI–PSL in Paris, France, since November 2020. He received his Ph.D. from the University of Northumbria in Newcastle, UK, in September 2020. His PhD work focused on utilizing passive smart surface coatings and active thin-film surface acoustic waves for anti-icing and de-icing on aluminum substrates. His current research focuses on single-molecule fluorescent microscopy of dense polymer melts, specifically PDMS polymers. Additionally, his work includes working on the grafting of fluorophores to PDMS chains.

Yihao Guo received his B.S. from Fujian Agriculture and Forestry University, China, in 2021. He is currently pursuing Ph.D. in the College of Mechanical and Vehicle Engineering, Hunan University, China. His research interests focus on SAW UV sensors.

Jaime del Moral (Sevilla, 1997) is a Ph.D. candidate of the SoundOfICE project at the Materials Science Institute of Seville (CSIC-US). He specializes in nanotechnology and implementing functional films into devices. He holds a double bachelor's degree in physics and materials science and a master's degree in microelectronics, from the University of Seville. His background combines thin films and nanostructures fabricated through plasma and vacuum and finite-element modeling for integrating bulk and surface acoustic waves for activation and sensing purposes. His thesis focuses on developing efficient solutions for ice accretion and sensing utilizing surface engineering of acoustic waves".

Stefan Jacob is a group leader specializing in acoustic sensors and measurement methods at the German National Metrology Institute (Physikalisch-Technische Bundesanstalt, PTB) in Braunschweig, Germany. He earned his Ph.D. in technical acoustics in 2017 from the Royal Institute of Technology (KTH) in Stockholm, Sweden. From 2021 to 2022, he was a postdoctoral researcher in the "Acoustic Microsystems" group at IFW Dresden, Germany. Dr. Jacob's research interests include the propagation of sound waves in both air and solids, advanced sensor technologies and sensor networks for sound measurement, and the innovative applications of sound waves in areas such as cleaning, de-icing, and energy harvesting.

Ana Borras (Seville, 1980) Since 2011 has been a tenured scientist at the Spanish National Scientific Council (CSIC). After earning her Ph.D. from the University of Seville in 2007, she worked at EMPA (Switzerland) on small-molecule nanowires and organic nanocomposite thin films. She leads the multifunctional one-dimensional nanomaterials research line at the Nanotechnology on Surfaces and Plasma Laboratory, focusing on complex hybrid and heterostructured materials. Ana Borras holds the ERC StG 3DScavengers grant and coordinates the EU project SoundOfICE, which applies functional surfaces and acoustic waves for de-icing and ice monitoring.

Agustin R. Gonzalez-Elipe is an "ad honorem" research professor of CSIC (National Research Council of Spain). His research activity focuses on the development of thin films for different advanced functional applications, plasma technology, and the use of advanced methods of material characterization. Recently he expanded his topics of interests to the field of de-icing using acoustic waves and piezoelectric materials. He has published several hundreds of scientific papers and some reviews and books. He collaborates actively with the industry and is the author of numerous patents, many of them transferred to companies.

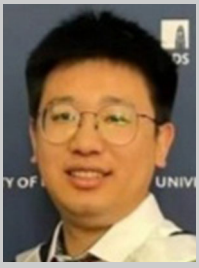

Jikai Zhang obtained his master's degree from the School of Chemical and Process Engineering, University of Leeds, UK, in 2019. He is currently a Ph.D. candidate under the supervision of Professor Richard Fu. His research is centered on drug delivery and tissue engineering using flexible acoustic waves.

Jian Zhou received his Ph.D. from Zhejiang University, China, in 2015. He is currently a professor from the College of Mechanical and Vehicle Engineering, Hunan University, China. Until now, he has published more than 90 academic articles. His current research interests focus on MEMS sensors.

Glen McHale is professor of Interfacial Science & Engineering at The University of Edinburgh, UK. He obtained his Ph.D. from the University of Nottingham, UK, and was a Royal Society European Research fellow at the Université de Pierre et Marie Curie, France, a professor at Nottingham Trent University and at University of Northumbria at Newcastle, UK. He has expertise in acoustic wave sensors and superhydrophobic, liquid-infused, and liquid-like surfaces. He has published over 250 journal papers with a Google Scholar index of 67 and over 17k citations. He is a fellow of the Royal Society for Arts, Manufactures & Commerce (RSA), the Institute of Physics (IoP) and the Higher Education Academy (HEA), and a senior member of the Institute of Electrical and Electronics Engineers (SMIEEE).

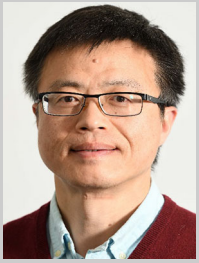

Yong-Qing Fu is currently a professor in University of Northumbria at Newcastle, UK. He obtained his Ph.D. from Nanyang technological University, Singapore, and was a research associate at University of Cambridge, UK, a lecturer in Heriot–Watt University at Edinburgh, and a reader at University of the West of Scotland, UK. He has extensive experience in smart thin films/coating materials, biomedical microdevices, energy materials, lab-on-chip, micromechanics, MEMS, nanotechnology, sensors, and microfluidics. He published over 500 journal papers with current Google scholar H-index of 84 and over 31 K citations. He is currently associate editor/editorial board member for a few international journals.